Bull Volcanol (2005) 67:391–414
DOI 10.1007/s00445-004-0377-3

RESEARCH ARTICLE

Catherine B. Lewis-Kenedi · Rebecca A. Lange · Chris M. Hall · Hugo Delgado-Granados

The eruptive history of the Tequila volcanic field, western Mexico: ages, volumes, and relative proportions of lava types

Received: 9 June 2003 / Accepted: 2 April 2004 / Published online: 6 August 2004

Abstract The eruptive history of the Tequila volcanic field (1600 km^2) in the western Trans-Mexican Volcanic Belt is based on ^{40}Ar/^{39}Ar chronology and volume estimates for eruptive units younger than 1 Ma. Ages are reported for 49 volcanic units, including Volcán Tequila (an andesitic stratovolcano) and peripheral domes, flows, and scoria cones. Volumes of volcanic units $\leq$1 Ma were obtained with the aid of field mapping, ortho aerial photographs, digital elevation models (DEMs), and ArcGIS software. Between 1120 and 200 kyrs ago, a bimodal distribution of rhyolite (~35 km^3) and high-Ti basalt (~39 km^3) dominated the volcanic field. Between 685 and 225 kyrs ago, less than 3 km^3 of andesite and dacite erupted from more than 15 isolated vents; these lavas are crystal-poor and show little evidence of storage in an upper crustal chamber. Approximately 200 kyr ago, ~31 km^3 of andesite erupted to form the stratocone of Volcán Tequila. The phenocryst assemblage of these lavas suggests storage within a chamber at ~2–3 km depth. After a hiatus of ~110 kyrs, ~15 km^3 of andesite erupted along the W and SE flanks of Volcán Tequila at ~90 ka, most likely from a second, discrete magma chamber located at ~5–6 km depth. The youngest volcanic feature (~60 ka) is the small andesitic volcano Cerro Tomasillo (~2 km^3). Over the last 1 Myr, a total of 128±22 km^3 of lava erupted in the Tequila volcanic field, leading to an average eruption rate of ~0.13 km^3/kyr. This volume erupted over ~1600 km^2, leading to an average lava accumulation rate of ~8 cm/kyr. The relative proportions of lava types are ~22–43% basalt, ~0.4–1% basaltic andesite, ~29–54% andesite, ~2–3% dacite, and ~18–40% rhyolite. On the basis of eruptive sequence, proportions of lava types, phenocryst assemblages, textures, and chemical composition, the lavas do not reflect the differentiation of a single (or only a few) parental liquids in a long-lived magma chamber. The rhyolites are geochemically diverse and were likely formed by episodic partial melting of upper crustal rocks in response to emplacement of basalts. There are no examples of mingled rhyolitic and basaltic magmas. Whatever mechanism is invoked to explain the generation of andesite at the Tequila volcanic field, it must be consistent with a dominantly bimodal distribution of high-Ti basalt and rhyolite for an 800 kyr interval beginning ~1 Ma, which abruptly switched to punctuated bursts of predominantly andesitic volcanism over the last 200 kyrs.

Keywords ^{40}Ar/^{39}Ar geochronology · GIS · Eruption rates · Aphyric andesites · Arc volcanism · Trans-Mexican Volcanic Belt

Electronic Supplementary Material Supplementary material is available in the online version of this article at http://dx.doi.org/10.1007/s00445-004-0377-3

Editorial responsibility: J. Donnelly-Nolan

C. B. Lewis-Kenedi · R. A. Lange (✉) · C. M. Hall
Department of Geological Sciences,
University of Michigan,
Ann Arbor, MI, 48109–1063, USA
e-mail: becky@umich.edu
Tel.: +1-734-7647421
Fax: +1-734-7634690

H. Delgado-Granados
Instituto de Geofísica, UNAM,
04510 DF Coyoacan, Mexico

Introduction

The Quaternary Tequila volcanic field, in the western Trans-Mexican arc, includes an andesitic stratovolcano (Volcán Tequila), as well as scoria cones, flows, and domes representing a complete compositional spectrum of basalt through rhyolite. An accurate assessment of possible petrogenetic links among the diverse compositions requires an eruptive history that includes the ages, volumes, and relative proportions of lava types. In this study, an intensive ^{40}Ar/^{39}Ar dating program is coupled to quantitative estimates of erupted volumes based on field mapping, ortho aerial photographs, digital elevation models, and geographic information system (GIS) soft-

ware. Such information on the chronology and volume of erupted lavas allows an examination of whether a time-progressive pattern in composition is observed, which can be used to test various models of magma differentiation. These data also constrain the length of time required to build a central volcano, which bears on the longevity of the underlying upper-crustal magma chamber(s) feeding the cone-building eruptions. When these cone-building durations are combined with a detailed study of the textures and phenocryst assemblages of the lavas erupted from large, central volcanoes versus small, peripheral vents, additional constraints on the timescale for upper crustal storage of arc magmas are obtained. On a broader scale, volumetric and chronological studies at volcanic arcs contribute to global compilations of eruption rates at subduction zones (Crisp 1984).

This study of the Tequila volcanic field is the second in a series designed to obtain a high-resolution record of the chronology and volume of erupted magma ($\leq$1 Ma) along the western Trans-Mexican arc. The results of this work can be compared with a similar study of the Ceboruco-San Pedro volcanic field (Frey et al 2004) located 75 km to the northwest. These adjacent volcanic fields have similar subduction parameters such as crustal thickness, age of the subducting slab, and rate of subduction. Therefore, a comparison of the eruptive history between the two adjacent volcanic fields within the last 1 Myr can be used to evaluate how much variation in eruptive volume and composition (relative proportions of lava types) occurs when subduction parameters are approximately constant.

Our primary goal was to identify and date all lavas erupted within the last 1 Myrs so that their individual and combined volumes could be evaluated. The difficulty in quantifying eruptive volumes at arc volcanic fields has long been recognized; factors include severe glacial erosion at high elevations and high latitudes (Singer et al 1997; Hildreth et al 2003) and/or extensive pyroclastic activity on volcanic islands, where the ash is lost to the marine environment (Druitt et al 1999). The Tequila volcanic field is ideal for a quantitative assessment of the volumes and proportions of different lava types owing to the absence of glacial erosion and the minor role of explosive volcanism. The rural, agricultural nature of the Tequila volcanic field provides roads and trails that allow access to all volcanic units. It is possible to see where flows have overlapped and to estimate flow thicknesses in the field. Moreover, many units have been mapped and characterized previously (Demant 1979; Harris 1986; Nixon et al 1987; Wopat 1990; Wallace and Carmichael 1994), and topographic maps, orthogonal aerial photographs, and digital elevation models (DEMs) are available for the entire area.

Tectonic setting

Volcán Tequila is one of eight major volcanic centers in the western Trans-Mexican Volcanic Belt (TMVB) (Fig. 1). The western TMVB is associated with subduction of the ~9 Myr old Rivera plate (Klitgord and Mammerickx 1982), whereas to the east the 12–18 Myr old Cocos plate subducts under North America. Seismic evidence suggests that the Rivera plate descends at an angle of 10° to a depth of 20 km, after which the angle steepens to 50° at 40 km; the subduction angle is unconfirmed below ~50 km owing to a lack of seismicity (Pardo and Suárez 1993). If the dip of 50° continues as the slab descends, then Volcán Tequila lies more than 200 km above the Wadati-Benioff zone, significantly further than the globally observed median depth of 125±38 km from the arc to the slab (Gill 1981). However, it is possible that the

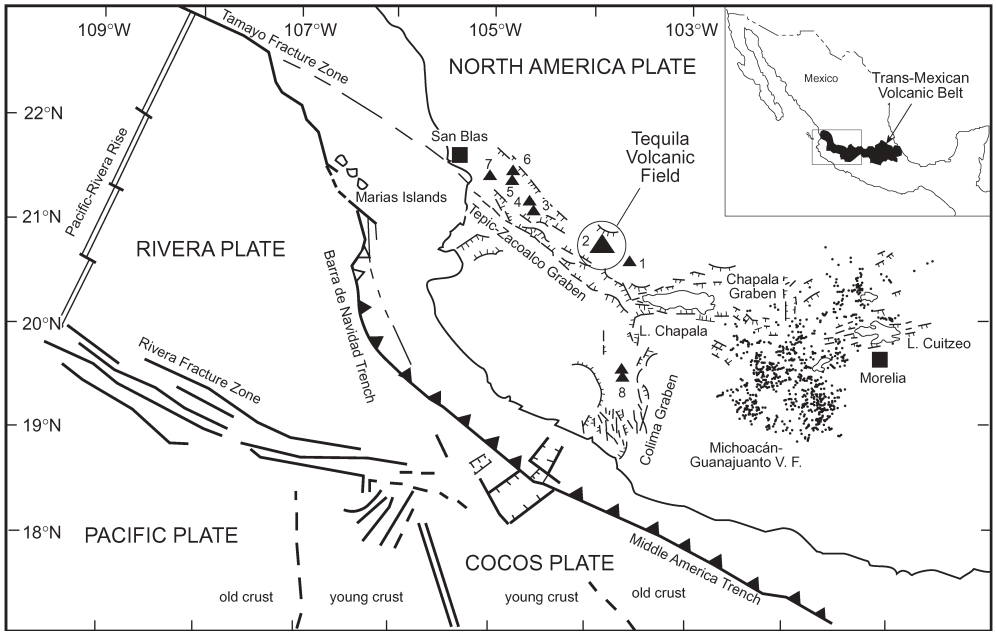

Fig. 1 Tectonic framework and overview of western Mexico, modified from Delgado-Granados (1993). Numbered triangles in the Tepic-Zacoalco and Colima grabens refer to central volcanoes: (1) Sierra La Primavera, (2) V. Tequila, (3) V. Ceboruco, (4) V. Tepetiltic, (5) V. Sangangüey, (6) V. Las Navajas, (7) V. San Juan, and (8) V. Colima-Nevado. The Michoacán-Guanajuanto volcanic field consists of numerous vents, represented by solid dots

slab angle becomes shallower with depth. The rate of subduction of the Rivera plate is estimated at 1.9±0.3 cm/yr along the western portion and 3.8±0.4 cm/yr in the east, at the Rivera-Cocos boundary (DeMets and Wilson 1997). Of special interest to this study is the evidence given by DeMets and Traylen (2000) that subduction of the Rivera plate ceased at ~2.6 Ma and then resumed normal convergence at ~1 Ma at an average rate of ~3.2 cm/yr. The crustal thickness in this region is estimated at 35–40 km from the gravity model of Urrutia-Fucugauchi and Flores-Ruis (1996).

Volcán Tequila is located within the Tepic-Zacoalco graben of western Mexico (Fig. 1), one of three grabens that intersect 50 km south-southwest of Guadalajara. Five andesitic stratovolcanoes, V. San Juan, V. Sangangüey, V. Tepetiltic, V. Ceboruco, and V. Tequila, as well as two silicic centers, Las Navajas and Sierra La Primavera, are confined to the Tepic-Zacoalco graben. Northwest-trending fractures and normal faults are common in the graben, and scoria cones frequently align along these northwest-trending lineaments (Allan et al 1991). Subduction-related and ocean-island type basaltic volcanism coexist in the Tepic-Zacoalco graben (Nelson and Livieres 1986; Allan et al 1991; Wallace et al 1992; Delgado-Granados 1993). Extensional tectonics are not uncommon at active margins as a consequence of low convergence rates (Otsuki 1989), as in the case of the active subduction system in Mexico (Delgado-Granados 1993).

The Tequila volcanic field

The andesitic stratovolcano of Volcán Tequila forms the center of the 1600 km^2 Tequila volcanic field and is surrounded by rhyolitic domes and flows, flanking andesitic flows, several scoria cones, and to the north, the basaltic Santa Rosa Plateau (Fig. 2). Volcán Tequila rises to 2920 m, 1800 m above the surrounding plains, and is constructed of andesite flows that are described in Wallace and Carmichael (1994). An erosional gully (300 m deep) cuts from the summit of the volcano to the northeast and has produced an alluvial fan that spreads over most of the northeastern flank. At the summit, there is a 300 m spine of silicic andesite (63 wt% SiO_2; Wallace and Carmichael 1994). Whereas Volcán Tequila is primarily an effusive volcano, minor ash deposits are found at the summit and remnants of small, dacitic airfall deposits are located on the northern (TQ23) and southwestern flanks (Fig. 2).

A small andesite volcano, Cerro Tomasillo, rests on the SE flank of Volcán Tequila (Fig. 3). A line of four, small dacite domes and associated flows are found immediately SE of C. Tomasillo. Fissure-fed flows of andesite blanket the W and SE flanks of Volcán Tequila and may have erupted along the same NW-SE lineament that includes the central vents of V. Tequila, Cerro Tomasillo, and the line of dacite domes (Fig. 2). Nine small scoria cones of andesite and dacite occur along the southern and western margins of V. Tequila, and seven scoria cones of basalt and basaltic andesite (and one additional cone of andesite) occur to the west, north, and east of the stratocone. Twelve rhyolitic domes and flows surround V. Tequila and are partly covered by younger andesitic flows; nine of these domes and flows are concentrated along the NW margin of V. Tequila. The rhyolites of the Tequila volcanic field have been described in detail, and seven of them were dated with the K-Ar method, by Harris (1986).

Immediately north of V. Tequila, fissure-fed flows of basalt (and minor basaltic andesite) comprise the Santa Rosa Plateau, which slopes ~1° to the N-NE and spans an area of ~190 km^2. These plateau lavas have been described in detail, and seven were dated with the K-Ar method, by Wopat (1990). The Santa Rosa Plateau underlies the agricultural lands between the northern base of Volcán Tequila and the southern rim of the Rio Grande de Santiago Canyon. This southern rim has an average elevation of ~1100 m, whereas the northern rim is ~700 m higher. As found elsewhere along the Rio Grande de Santiago (Nieto-Obregón et al 1985; Wopat 1990), basaltic lavas have periodically filled and flooded the canyon, causing the river to re-incise through the flows. It is likely that most, although not all, of the capping basalt lavas that form the primary cover to the Santa Rosa Plateau were erupted from fissures located within the canyon, along the same NW-SE lineament that the Rio Grande de Santiago follows. The capping basalts show no evidence of individual flow margins and/or pressure ridges, which suggests that they flooded the canyon and overflowed onto a flat-lying lacustrine lake deposit (exposed beneath the basalts on the southern wall of the Rio Grande de Santiago Canyon). Because the northern rim of the canyon was higher than the southern rim, flows that filled the canyon overflowed the southern rim, and formed the Santa Rosa Plateau to the south. The current shallow dip of the Santa Rosa Plateau toward the north is likely the result of continued normal faulting since the emplacement of the basalts. Normal faulting along this segment of the Rio Grande de Santiago Canyon has offset a 5.5 Ma ash-flow tuff on the northern wall by ~450 m (Nieto-Obregón et al 1985), and it likely accounts for the higher elevation of the northern rim of the canyon.

Several additional studies have contributed information on the Tequila volcanic field. Demant (1979) provided the first detailed geological study of the area, including the petrography and chemistry of several lavas from the area. Nieto-Obregón et al (1985) described the stratigraphy and structure of this region and reported both new K-Ar dates and those of others, including Damon et al (1979). Nixon et al (1987) revised the geologic map, and reported chemical analyses and K-Ar ages on three samples: an andesite from the upper part of V. Tequila, a basalt from the Santa Rosa Plateau, and a dacitic flow north of the town of Tequila.

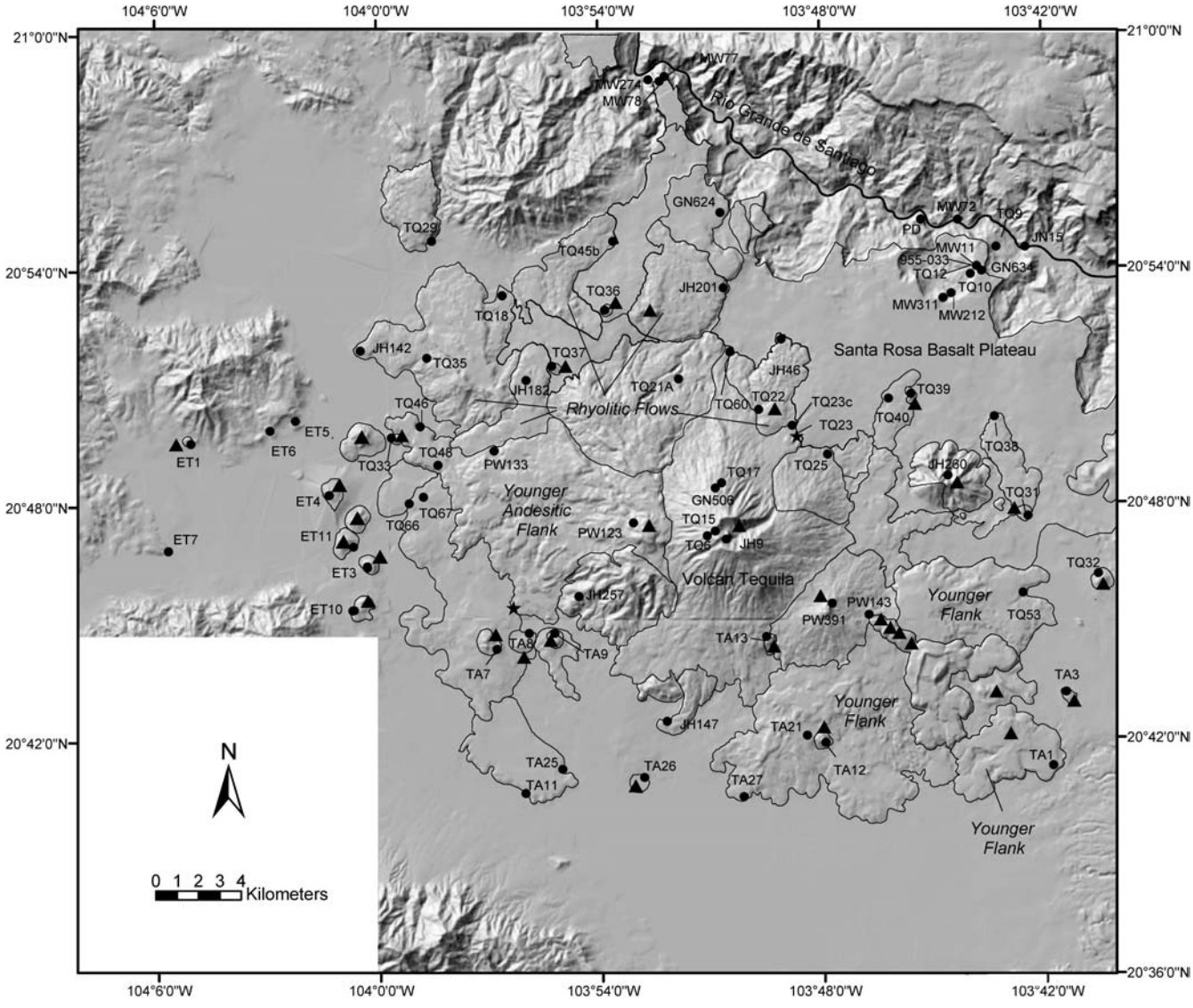

Fig. 2 Digital elevation model-based image of the Tequila volcanic field with the geologic units outlined as on the geologic map (Fig. 3). Solid circles represent locations of all dated and/or analyzed samples. The two solid stars are locations of dacitic airfall pumice. Samples TQ, TA, and ET are from this study (TEQ, TAL, and ETZ in Tables 1a–1d, 2, 3, 4, 5, 6, 7). PW labels are samples that we dated from the study of Wallace and Carmichael (1994). Dated samples from other authors are as follows: MW, Wopat (1990); GN, Nixon et al (1987); JH, Harris (1986); 995–033, Gilbert et al (1985); JN, Nieto-Obregón et al (1985); PD, Damon et al (1979). Solid triangles represent eruptive vents; symbols may be to the side of the actual vent to accommodate the labels of sample locations

Composition and mineralogy of lava types

Fifty samples were analyzed for major element chemistry by inductively coupled plasma (ICP) analysis and for trace and rare earth element chemistry by ICP mass spectrometry (ICP-MS) at Activation Laboratories in Ancaster, Ontario (Tables 1a–1d, 2, 3, 4). The lavas are classified on the basis of silica content as follows: basalt (<52 wt% SiO_2), basaltic andesite (52–56 wt% SiO_2), andesite (58–64 wt% SiO_2), dacite (65–69 wt% SiO_2), and rhyolite ($\geq$70 wt% SiO_2). Modal abundances were determined by point counts with >1400 points (Tables 1a–1d, 2, 3, 4). Crystals >0.3 mm are classified as phenocrysts, microphenocrysts are 0.03–0.3 mm, and groundmass is <0.03 mm. Whole-rock analyses and thin sections of collected samples were used in constructing the geologic map shown in Fig. 3.

Basalts and basaltic andesites

Basalt and minor basaltic andesite comprise the fissure-fed Santa Rosa Plateau as well as scoria cones and associated flows erupted from vents on top of the plateau. Both the basalts and basaltic andesites are rich in TiO_2 (2.0–2.6 and 1.3–2.1 wt.%, respectively) (Tables 1a–1d, 2, 3, 4). These mafic lavas contain phenocrysts of olivine+plagioclase±augite. One basaltic andesite (TEQ33) from a small

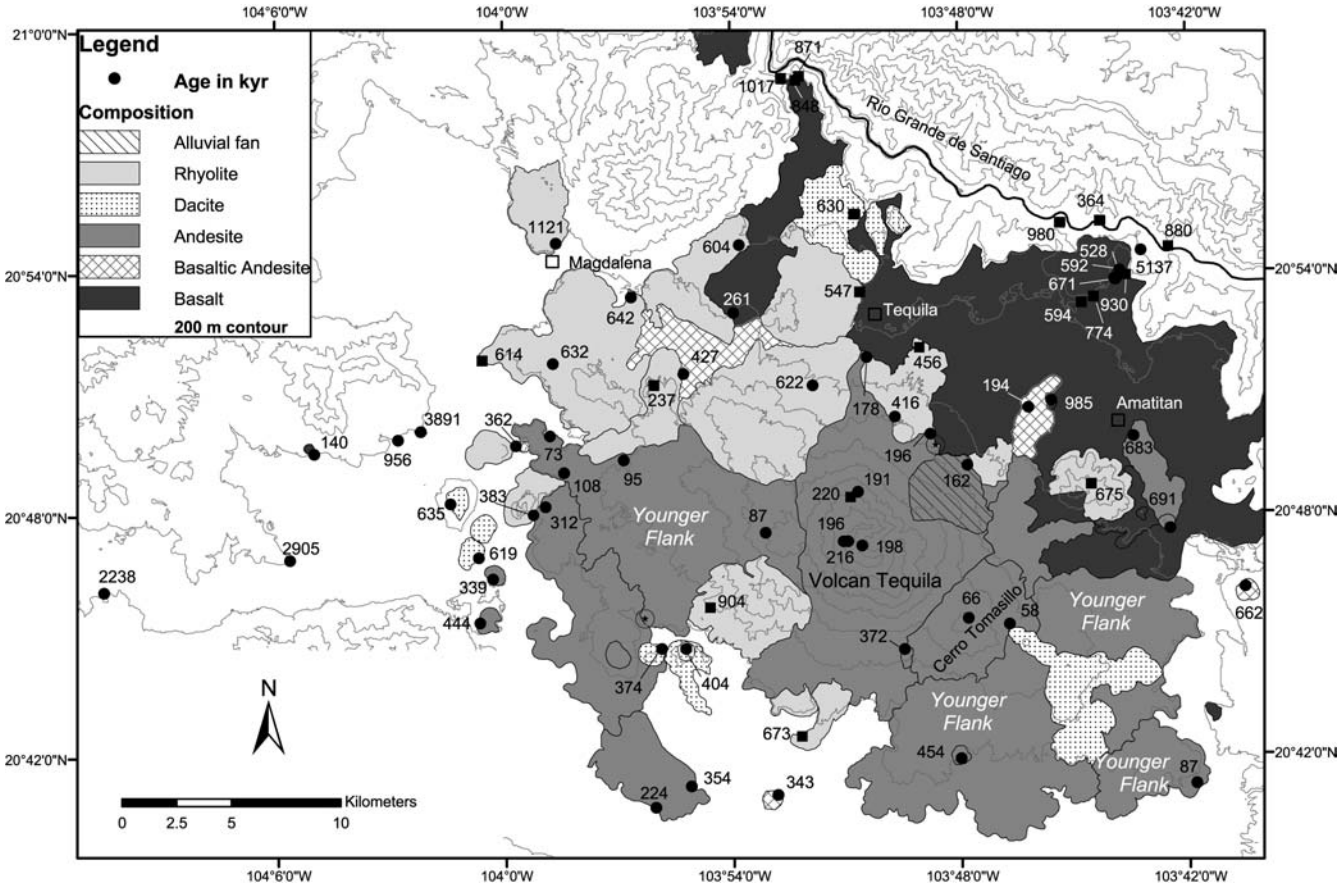

Fig. 3 Geologic map of the Tequila volcanic field. Solid circles (dots) represent locations for all dated samples, which are labeled with ages in kyr. Solid squares represent samples dated by other authors; see Fig. 2. Error information for each age is in Tables 5, 6, 7. The dacite outcrop of TEQ66 (Fig. 2) is too small to be shown on this map

scoria cone also contains phenocrysts of hornblende. The olivine basalts that filled and flooded the canyon (like TEQ10, TEQ12) have a characteristic petrographic texture of a coarsely crystalline groundmass combined with abundant plagioclase microphenocrysts (~18–24 vol%), which is in marked contrast to similar olivine basalts erupted as scoria cones or flows on top of the Santa Rosa Plateau (such as ETZ1, TEQ39). These samples have a fine-grained groundmass with far less abundant microphenocrysts of plagioclase (3–6 vol%), although their bulk compositions are similar to those from the Santa Rosa plateau.

Andesites

Andesites in the Tequila volcanic field are divided into four categories: (1) the main edifice of Volcán Tequila, (2) younger flank flows along the SE and W margins of V. Tequila, (3) the small volcano of Cerro Tomasillo, and (4) peripheral scoria cones and flows. The lavas from V. Tequila span a range in silica (59–64 wt%; Tables 1a–1d, 2, 3, 4) similar to the range seen in the younger flank lavas (59–64 wt%; Tables 1a–1d, 2, 3, 4), and both groups have TiO_2 concentrations that vary from 0.9–0.6 wt%. Both groups display mineralogy and textures typical of those seen in large, andesitic stratovolcanoes; they are phenocryst-rich (10–25%), with plagioclase and two pyroxene assemblages. Plagioclase is the most abundant phenocryst and often displays complex zoning, as well as inner cores (sometimes bands) that are riddled with melt inclusions (Wallace and Carmichael 1994). All of the younger lavas along the west flank of V. Tequila additionally contain hornblende phenocrysts. The flows from Cerro Tomasillo that are dated in this study are similar in most respects to those from V. Tequila (Wallace and Carmichael 1994). Flank and central flows contain abundant Fe-Ti oxides in the groundmass that are commonly too small to be categorized as microphenocrysts.

The peripheral flows and scoria cones of andesite, not associated with the central vent or younger flank flows of V. Tequila, are texturally and compositionally distinct. Although their range in silica is similar to that for the samples from V. Tequila and its younger flanks, the peripheral andesites contain higher concentrations of both TiO_2 (1.2–1.4 wt%) and total iron (Tables 1a–1d, 2, 3, 4). These flows are remarkably crystal-poor (3–12 vol%) and include sparse euhedral prisms of plagioclase with inner cores that are often riddled with melt inclusions. Orthopyroxene and augite are always present, and horn-

Table 1a Whole-rock major element (wt %) and trace element (ppm) composition and modal analyses (%) of dated samples

	Basalts						Basaltic andesites					
	Peripheral flows and cones around Volcán Tequila						Peripheral flows and cones around Volcán Tequila					
	TEQ 12	TEQ 10	TAL 3	ETZ 1	TEQ 36	TEQ 39	ETZ 6	TAL 26	TEQ 40	TEQ 37	TEQ 32	TEQ 33
	lava flow	lava flow	cone	cone	cone	cone	lava flow	lava flow	cone	cone	cone	cone
SiO_2	49.0	49.1	49.5	50.0	50.5	50.6	52.6	53.2	53.9	54.0	55.7	56.0
TiO_2	2.46	2.46	2.04	2.31	2.33	2.59	1.29	1.72	1.39	1.77	1.74	1.61
Al_2O_3	16.2	15.8	16.5	15.8	16.1	15.7	17.1	16.5	17.9	16.4	16.2	16.6
FeO*	10.9	11.2	10.2	9.1	10.1	10.5	7.14	8.83	7.27	8.05	8.13	7.92
MnO	0.19	0.19	0.17	0.19	0.18	0.16	0.17	0.17	0.12	0.14	0.16	0.13
MgO	5.55	5.76	5.76	5.45	5.28	3.44	5.78	4.52	3.76	4.29	3.25	3.28
CaO	8.92	8.91	9.00	8.11	7.43	6.97	8.28	7.22	7.70	7.15	6.34	6.56
Na_2O	3.76	3.79	3.56	3.73	3.48	3.59	3.64	3.85	3.62	3.82	4.13	4.10
K_2O	1.14	1.12	1.01	1.66	1.69	1.73	1.26	1.91	1.71	2.19	2.14	1.94
P_2O_5	0.52	0.53	0.43	0.99	1.06	0.61	0.39	0.92	0.36	0.60	0.65	0.55
LOI	-0.17	-0.59	0.11	0.18	1.19	1.46	0.39	0.24	0.48	0.87	0.60	0.60
Total	98.54	98.28	98.21	97.56	99.36	97.33	97.96	99.10	98.16	99.22	99.09	99.26
Zr	192	185	175	205	262	210	171	320	175	133	113	207
Ba	358	337	414	684	923	670	655	826	626	824	795	791
Age (± 1σ)	592 ± 20	671 ± 13	not dated	140 ± 12	261 ± 11	985 ± 48	956 ± 48	343 ± 38	194 ± 15	427 ± 20	662 ± 60	362 ± 13
Plag ph	8.5	6.3	4.2	5.0	0.7	0.2	4.8	22.0	23.4	2.9	1.0	3.1
Plag mph	23.9	18.5	5.8	5.4	3.7	2.5	5.6	10.0	7.0	7.9	2.8	7.4
Opx ph	-	-	-	-	-	-	-	-	-	-	-	-
Opx mph	-	-	-	-	-	-	-	-	-	-	-	-
Cpx ph	-	-	-	-	-	-	1.0	-	2.4	-	-	0.4
Cpx mph	0.2	0.7	-	-	-	-	-	-	2.5	-	0.3	1.4
Ol ph	5.5	4.5	2.6	3.3	0.2	-	6.6	0.3	1.2	0.7	2.5	0.2
Ol mph	3.5	4.3	2.6	0.5	3.9	0.5	0.5	3.6	1.0	1.3	0.7	0.8
Hbd ph	-	-	-	-	-	-	-	-	-	-	-	-
Hbe mph	-	-	-	-	-	-	-	-	-	-	-	0.8
Oxide	0.5	0.6	-	-	0.9	0.6	0.4	-	0.2	-	-	0.5
Xls	42.1	34.9	15.2	14.2	9.4	3.8	18.9	35.9	37.7	12.8	7.3	14.6
Gmass	57.9	65.1	84.8	85.8	90.6	96.2	81.1	64.1	62.3	87.2	92.7	85.4

Notes: FeO* is total Fe as FeO. Modal analyses are given in vol. % and were determined by point counting >1500 points. Abbreviations: Ph = phenocrysts (>0.3 mm); Mph = microphenocrysts (>0.03 mm); Xls = total crystals; Gmass = groundmass; Plag = plagioclase, Opx = orthopyroxene, Cpx = clinopyroxene, Hbd = hornblende. Major and trace elements were analyzed by ICP and ICP-MS at Activation Laboratories of Ancaster, Ontario. Errors are ± 0.01% relative for major elements, ± 5 ppm for Zr, and ± 3 ppm for Ba. Latitude and longitude are given in Table 2
Preferred ages from Table 2 are given here to help correlate samples between tables and maps

blende is found in all peripheral lavas with $\geq$59.5 wt% SiO_2. The hornblende is often completely surrounded by an opaque reaction rim (opacite). Rare xenocrysts of sieve-textured plagioclase with no rims are found in one sample (TAL13).

Dacites

The most prominent occurrence of dacite is the line of four domes and associated flows immediately SE of Cerro Tomasillo. One of the domes was analyzed by wet chemistry and contains 69 wt% SiO_2 and 0.4 wt% TiO_2 (Harris 1986). The domes contain 10% phenocrysts of plagioclase, hornblende, and minor orthopyroxene (sample Q39 from Wallace and Carmichael 1994). Dacitic pumice (TEQ23) from a small airfall deposit contains phenocrysts of hornblende, plagioclase, and trace amounts of orthopyroxene. The source may be the central vent of V. Tequila, prior to the eruption of the main andesitic cone. Additional occurrences of dacite include five glassy scoria cones and a few dacite flows (like TEQ66), all of which are peripheral to V. Tequila. These cones range from 65 to 68 wt% SiO_2 and, like the peripheral andesitic scoria cones, are notably crystal-poor (4–10 vol%) and are relatively rich in TiO_2 (0.9–0.5 wt%). The phenocrysts include clear euhedral prisms of plagioclase (some of which have inner cores with melt inclusions) in addition to orthopyroxene, sparse augite, and opacitic hornblende.

Rhyolites

The rhyolitic domes and flows in the Tequila volcanic field include peraluminous, metaluminous, and peralkaline varieties that range from 70 to 76.5 wt% SiO_2 (Harris 1986; wet chemical analyses by ISE Carmichael). Domes consist of light-colored, porphyritic flows, often with obsidian streaks, that contain 0–5 vol% phenocrysts of plagioclase±sanidine±augite in fine-grained groundmass; no quartz phenocrysts were found in the samples collected by Harris (1986) or in the seven samples collected and examined in this study. For our samples, SiO_2 contents range from 74 to 76.5 wt% (Tables 1a–1d, 2, 3, 4; after LOI correction for TEQ29 pumice). Four of the samples have no phenocrysts or microphenocrysts. The remaining two samples (TEQ20 and TEQ21a) contain sparse phe-

Table 1b Whole-rock major element (wt %) and trace element (ppm) composition and modal analyses (%) of dated samples

	Andesites					Andesites					Andesites				
	Main edifice of Volcán Tequila					Younger W flank flows of V. Tequila					Younger SE flank flows of V. Tequila				
	TEQ 15	TEQ 23c	TEQ 25	TEQ 60	TEQ 17[a]	TEQ 6	JH009	PW 133	TEQ 48	TEQ 46	PW 123	TAL 27	TAL 21	TAL 1	TEQ 53
	flow	flow	flow	flow	flow	flow	spine	flow	flow	flow	flow	flow	flow	flow	flow
SiO_2	57.6	60.8	61.2	61.6	62.7	63.1	62.9	57.0	58.6	58.9	63.8	59.1	59.4	60.6	61.0
TiO_2	0.78	0.75	0.77	0.76	0.69	0.69	0.75	1.00	0.98	1.02	0.67	0.87	0.87	0.77	0.74
Al_2O_3	18.9	16.6	17.0	16.6	16.6	16.4	16.9	16.8	16.9	17.2	16.4	17.2	17.2	17.3	17.0
FeO*	5.05	4.76	4.94	4.63	3.85	4.36	4.67	5.84	5.80	5.92	4.22	5.60	5.56	5.17	4.96
MnO	0.09	0.08	0.09	0.08	0.08	0.08	0.08	0.10	0.11	0.11	0.08	0.11	0.11	0.10	0.09
MgO	2.91	3.09	2.93	2.90	2.63	2.52	2.91	3.88	3.65	3.49	2.30	3.39	3.37	3.06	2.84
CaO	6.11	5.81	5.93	5.76	5.30	5.54	5.35	7.14	6.26	6.25	4.55	6.34	6.35	6.06	5.82
Na_2O	3.44	3.70	3.74	3.73	3.54	3.90	3.76	3.81	3.68	4.11	3.57	3.81	3.78	4.01	3.72
K_2O	1.68	2.28	2.12	2.16	2.34	2.19	2.22	2.48	2.50	1.99	2.68	1.89	2.09	1.97	2.39
P_2O_5	0.17	0.19	0.24	0.18	0.13	0.15	0.18	0.31	0.31	0.32	0.12	0.32	0.32	0.25	0.23
LOI	2.53	1.24	0.90	1.05	1.75	0.55	-	-	0.48	-0.03	-	0.71	0.66	0.41	0.77
Total	99.26	99.25	99.79	99.42	99.58	99.38	99.76	98.38	99.23	99.30	98.37	99.30	99.77	99.72	99.51
Zr	155	155	155	168	145	137	145	227	236	234	175	207	196	184	189
Ba	920	736	736	789	713	776	799	712	785	792	830	677	694	687	717
Age (± 1σ)	196 ± 8	196 ± 19	162 ± 20	178 ± 8	191 ± 13	216 ± 11	198 ± 11	95 ± 42	108 ± 27	73 ± 24	87 ± 12	not dated	not dated	87 ± 11	not dated
Plag ph	6.2	13.3	2.6	10.1	14.5	5.9	1.9	10.1	6.9	5.5	9.3	7.8	0.5	8.1	8.7
Plag mph	10.7	7.2	14.1	5.3	6.7	11.4	17.7	3.1	5.0	9.4	1.7	10.2	13.1	3.9	9.3
Opx ph	1.5	2.4	1.5	3.2	2.0	1.2	0.2	2.8	1.0	1.2	0.9	0.9	0.5	1.1	2.4
Opx mph	1.5	2.3	0.7	0.9	1.4	5.5	1.4	0.8	2.1	0.8	1.5	1.1	0.5	0.9	1.5
Cpx ph	1.0	1.7	0.3	2.0	1.2	1.0	-	2.8	1.4	2.0	-	1.1	0.3	2.0	0.6
Cpx mph	0.6	0.6	1.3	1.6	0.2	0.5	0.3	0.4	2.0	1.2	0.1	-	0.1	1.7	1.2
Ol ph	-	-	-	-	-	-	-	-	-	-	-	-	-	-	-
Ol mph	-	-	-	-	-	-	-	-	-	-	-	-	-	-	-
Hbd ph	-	-	-	-	-	-	-	2.5	0.5	1.2	2.1	-	-	-	-
Hbe mph	-	-	-	-	-	-	-	0.8	0.3	2.6	1.0	-	-	trace	-
Oxide	0.5	0.2	0.8	0.3	0.1	0.1	trace	0.3	0.6	1.5	0.3	0.6	0.3	-	0.5
Xls	22.0	27.7	21.3	23.4	26.1	25.6	21.5	23.6	19.8	25.4	16.9	21.7	15.3	17.7	23.7
Gmass	78.0	72.3	78.7	76.6	73.9	74.4	78.5	76.4	80.2	74.6	83.1	78.3	84.7	82.3	76.3

Notes: Same as Table 1a. Analyses and modes for PW samples are from Wallace and Carmichael 1994; JH009 is the spine (sample 108 in Wallace and Carmichael 1994)
[a] Note the large LOI on these samples

Table 1c Whole-rock major element (wt %) and trace element (ppm) composition and modal analyses (%) of dated samples

	Dacite	Andesite					Andesite						
	V. Tequila?	Cerro Tomasillo					Older peripheral flows and cones around Volcán Tequila						
	TEQ 23[a]	PW 391	PW 143	TEQ 31	TEQ 38	ETZ 10a	TEQ 67	ETZ 3	TAL 11	TAL 25	TAL 7	TAL 13	TAL 12
	pumice	flow	flow	cone	flow	cone	flow	cone	flow	flow	cone	cone	cone
SiO_2	63.6	60.3	62.2	58.1	58.2	58.8	59.0	59.4	59.4	59.7	59.8	60.7	62.0
TiO_2	0.62	0.81	0.74	1.18	1.15	1.46	1.28	1.23	1.42	1.44	1.42	1.27	1.14
Al_2O_3	15.8	17.7	16.9	17.1	16.9	16.1	16.7	16.5	16.4	16.3	16.2	16.2	16.2
FeO*	3.33	5.37	4.51	6.61	6.51	7.24	6.04	6.42	6.40	6.32	6.51	6.16	5.19
MnO	0.06	0.10	0.08	0.12	0.11	0.12	0.11	0.11	0.12	0.12	0.12	0.11	0.11
MgO	1.10	3.11	2.29	3.11	3.05	2.78	3.11	3.00	2.54	2.40	2.44	2.51	2.50
CaO	3.47	6.05	4.95	6.14	6.12	5.81	6.11	6.01	5.38	5.19	5.32	5.39	5.25
Na_2O	3.19	4.06	3.25	4.18	3.99	4.28	4.12	4.20	4.16	4.13	4.49	4.37	4.28
K_2O	2.50	1.91	2.93	1.91	2.06	2.20	2.05	2.07	2.57	2.79	2.31	2.35	2.44
P_2O_5	0.16	0.27	0.19	0.31	0.32	0.38	0.39	0.43	0.49	0.52	0.52	0.41	0.36
LOI	6.04			0.43	0.77	-0.23	0.10	0.02	0.62	0.44	-0.01	-0.19	-0.01
Total	99.80	99.66	97.98	99.17	99.23	98.91	98.98	99.40	99.60	99.37	99.08	99.26	99.48
Zr	189	176	188	170	151	168	187	182	222	236	206	156	191
Ba	930	628	808	721	740	685	734	776	829	874	776	832	766
Age (± 1σ)	not dated	66 ± 20	58 ± 10	691 ± 26	683 ± 32	444 ± 140	312 ± 32	339 ± 35	224 ± 11	354 ± 15	not dated	372 ± 18	454 ± 32
Plag ph	1.0	1.0	10.6	0.8	0.3	0.8	1.4	1.9	1.0	1.1	0.5	1.0	2.6
Plag mph	0.3	7.8	1.9	4.3	6.5	2.2	3.1	1.3	4.5	0.6	9.4	1.9	3.2
Opx ph	0.1	-	1.0	-	0.5	-	-	0.8	0.3	0.5	0.6	0.4	0.2
Opx mph	0.4	0.4	1.3	-	-	-	0.3	0.1	-	0.1	0.1	0.2	0.8
Cpx ph	-	-	0.5	0.2	-	-	-	0.2	-	0.1	-	0.7	0.6
Cpx mph	0.2	0.1	0.2	0.3	0.3	0.3	0.3	1.0	0.5	-	0.4	-	1.2
Ol ph	-	-	-	-	-	-	-	-	-	-	-	0.4	0.3
Ol mph	-	-	-	-	-	-	-	-	-	-	-	-	-
Hbd ph	1.2	-	-	-	-	-	-	-	-	0.7	-	1.3	-
Hbe mph	0.5	-	0.1	-	-	-	-	-	0.9	0.5	0.7	0.4	trace
Oxide	-	-	trace	1.0	0.7	-	0.4	-	0.5	0.6	0.6	0.2	-
Xls	3.7	9.3	15.6	6.6	8.3	3.3	5.5	5.3	7.7	4.2	12.3	4.6	8.9
Gmass	96.3	90.7	84.4	93.4	91.7	96.7	94.5	94.7	92.3	95.8	87.7	95.4	91.1

Notes: Same as Table 1a.

[a] Note the large LOI on these samples. Analyses and modes for PW samples are from Wallace and Carmichael 1994

Table 1d Whole-rock major element (wt %) and trace element (ppm) composition and modal analyses (%) of dated samples

	Dacites					Rhyolites					Flows >1 Ma				
	Older peripheral flows and cones around V. Tequila														
	TAL 8	TAL 9	ETZ 11	ETZ 4	TEQ 66	TEQ 29[a]	TEQ21a	TEQ 18	TEQ 22	TEQ 45b	TEQ 35	ETZ 7	ETZ 5	TEQ 9[a]	ETZ 2[a]
	cone	cone	cone	cone	flow	pumice	obsidian	obsidian	obsidian	obsidian	obsidian	obsidian	flow	tuff	flow
SiO_2	64.6	66.3	66.6	67.5	68.4	73.7	74.1	74.1	74.5	75.0	75.4	75.8	55.2	55.2	61.4
TiO_2	0.93	0.77	0.71	0.53	0.68	0.09	0.15	0.11	0.15	0.12	0.11	0.16	1.79	1.21	0.67
Al_2O_3	15.7	15.4	15.5	15.3	14.6	12.6	13.3	12.3	13.4	13.1	12.6	13.1	16.8	16.2	17.4
FeO*	4.27	3.95	3.55	3.10	3.07	1.21	1.46	1.35	1.32	1.32	1.34	1.15	8.65	5.69	4.72
MnO	0.09	0.08	0.09	0.10	0.07	0.05	0.06	0.05	0.04	0.06	0.06	0.04	0.14	0.13	0.07
MgO	1.33	1.56	0.94	0.50	0.92	0.05	0.11	0.08	0.13	0.07	0.06	0.17	2.44	2.40	2.07
CaO	3.46	3.55	2.57	1.48	2.33	0.48	0.51	0.42	0.63	0.42	0.39	0.86	5.82	5.48	5.89
Na_2O	4.75	4.48	5.06	5.47	4.44	3.69	4.61	4.35	4.50	4.67	4.45	4.20	4.62	2.79	4.00
K_2O	3.00	3.30	3.65	4.29	3.89	4.60	4.83	4.62	4.71	4.77	4.66	4.31	1.99	1.71	1.49
P_2O_5	0.32	0.23	0.22	0.13	0.22	0.02	0.03	0.02	0.03	0.02	0.02	0.04	0.58	0.37	0.19
LOI	0.28	0.02	0.16	0.52	-0.06	3.81	1.14	0.67	0.87	0.20	1.25	0.43	1.08	8.12	1.59
Total	98.71	99.70	99.10	98.84	98.59	100.33	100.33	98.07	100.26	99.80	100.31	100.24	99.06	99.33	99.50
Zr	249	259	404	811	237	163	263	234	183	254	228	157	251	207	129
Ba	913	927	957	1370	852	166	342	55	940	81	53	911	820	823	666
Age (± 1σ)	374 ± 11	404 ± 15	619 ± 8	635 ± 4	383 ± 4	1121 ± 149	622 ± 3	642 ± 6	416 ± 3	604 ± 3	632 ± 8				
Plag ph	1.9	1.1	2.3	-	1.2	9.0	0.6	-	-	-	-				
Plag mph	3.4	1.0	6.0	3.4	6.0	0.5	0.3	-	-	-	-				
Opx ph	-	0.3	-	1.8	-	-	-	-	-	-	-				
Opx mph	0.2	0.1	-	0.1	0.3	-	-	-	-	-	-				
Cpx ph	0.7	0.1	-	0.1	0.5	0	-	-	-	-	-				
Cpx mph	0.3	0.2	0.2	0.2	0.3	-	-	-	-	-	-				
Hbd ph	1.2	-	1.3	-	-	0.1	-	-	-	-	-				
Hbd mph	0.2	0.9	0.4	-	1.5	-	-	-	-	-	-				
Alk fspar ph	-	0.2	-	-	-	3.9	1.2	-	-	-	-				
Alk fspar mph	-	-	-	-	-	-	0.4	-	-	-	-				
Quartz ph	-	0.2	-	-	-	-	-	-	-	-	-				
Xls	7.9	4.1	10.2	5.6	9.8	13.5	2.5	0.0	0.0	0.0	0.0				
Gmass	92.1	95.9	89.8	94.4	90.2	86.5	97.5	100.0	100.0	100.0	100.0				

Notes: Same as Table 1a. Abbreviations: Alk fspar = alkali feldspar.
[a] Note the large LOI on these samples

Table 2 Whole-rock major element (wt%) and trace element (ppm) composition and modal analyses (%) of dated andesite samples

	Main edifice of Volcán Tequila							Younger W flank flows of V. Tequila				Younger SE flank flows of V. Tequila			
	TEQ 15	TEQ 23c	TEQ 25	TEQ 60	TEQ 17[a]	TEQ 6	JH009	PW 133	TEQ 48	TEQ 46	PW 123	TAL 27	TAL 21	TAL 1	TEQ 53
	flow	flow	flow	flow	flow	flow	spine	flow	flow	flow	flow	flow	flow	flow	flow
SiO_2	57.6	60.8	61.2	61.6	62.7	63.1	62.9	57.0	58.6	58.9	63.8	59.1	59.4	60.6	61.0
TiO_2	0.78	0.75	0.77	0.76	0.69	0.69	0.75	1.00	0.98	1.02	0.67	0.87	0.87	0.77	0.74
Al_2O_3	18.9	16.6	17.0	16.6	16.6	16.4	16.9	16.8	16.9	17.2	16.4	17.2	17.2	17.3	17.0
FeO[a]	5.05	4.76	4.94	4.63	3.85	4.36	4.67	5.84	5.80	5.92	4.22	5.60	5.56	5.17	4.96
MnO	0.09	0.08	0.09	0.08	0.08	0.08	0.08	0.10	0.11	0.11	0.08	0.11	0.11	0.10	0.09
MgO	2.91	3.09	2.93	2.90	2.63	2.52	2.91	3.88	3.65	3.49	2.30	3.39	3.37	3.06	2.84
CaO	6.11	5.81	5.93	5.76	5.30	5.54	5.35	7.14	6.26	6.25	4.55	6.34	6.35	6.06	5.82
Na_2O	3.44	3.70	3.74	3.73	3.54	3.90	3.76	3.81	3.68	4.11	3.57	3.81	3.78	4.01	3.72
K_2O	1.68	2.28	2.12	2.16	2.34	2.19	2.22	2.48	2.50	1.99	2.68	1.89	2.09	1.97	2.39
P_2O_5	0.17	0.19	0.24	0.18	0.13	0.15	0.18	0.31	0.31	0.32	0.12	0.32	0.32	0.25	0.23
LOI	2.53	1.24	0.90	1.05	1.75	0.55	-	-	0.48	–0.03	-	0.71	0.66	0.41	0.77
Total	99.26	99.25	99.79	99.42	99.58	99.38	99.76	98.38	99.23	99.30	98.37	99.30	99.77	99.72	99.51
Zr	155	155	155	168	145	137	145	227	236	234	175	207	196	184	189
Ba	920	736	736	789	713	776	799	712	785	792	830	677	694	687	717
Age (±1σ)	196±8	196±19	162±20	178±8	191±13	216±11	198±11	95±42	108±27	73±24	87±12	not dated	not dated	87±11	not dated
plag ph	6.2	13.3	2.6	10.1	14.5	5.9	1.9	10.1	6.9	5.5	9.3	7.8	0.5	8.1	8.7
plag mph	10.7	7.2	14.1	5.3	6.7	11.4	17.7	3.1	5.0	9.4	1.7	10.2	13.1	3.9	9.3
opx ph	1.5	2.4	1.5	3.2	2.0	1.2	0.2	2.8	1.0	1.2	0.9	0.9	0.5	1.1	2.4
opx mph	1.5	2.3	0.7	0.9	1.4	5.5	1.4	0.8	2.1	0.8	1.5	1.1	0.5	0.9	1.5
cpx ph	1.0	1.7	0.3	2.0	1.2	1.0	-	2.8	1.4	2.0	-	1.1	0.3	2.0	0.6
cpx mph	0.6	0.6	1.3	1.6	0.2	0.5	0.3	0.4	2.0	1.2	0.1	-	0.1	1.7	1.2
ol ph	-	-	-	-	-	-	-	-	-	-	-	-	-	-	-
ol mph	-	-	-	-	-	-	-	-	-	-	-	-	-	-	-
hbd ph	-	-	-	-	-	-	-	2.5	0.5	1.2	2.1	-	-	-	-
hbe mph	-	-	-	-	-	-	-	0.8	0.3	2.6	1.0	-	-	trace	-
oxide	0.5	0.2	0.8	0.3	0.1	0.1	trace	0.3	0.6	1.5	0.3	0.6	0.3	-	0.5
xls	22.0	27.7	21.3	23.4	26.1	25.6	21.5	23.6	19.8	25.4	16.9	21.7	15.3	17.7	23.7
gmass	78.0	72.3	78.7	76.6	73.9	74.4	78.5	76.4	80.2	74.6	83.1	78.3	84.7	82.3	76.3

Notes: Same as Table 1a. Analyses and modes for PW samples are from Wallace and Carmichael (1994); JH009 is the spine (sample 108 in Wallace and Carmichael 1994). [a] Note the large LOI on these samples

Table 3 Whole-rock major element (wt%) and trace element (ppm) composition and modal analyses (%) of dated andesite samples

	Andesite		Andesite									
	Cerro Tomasillo		Older peripheral flows and cones around Volcán Tequila									
	PW 391	PW 143	TEQ 31	TEQ 38	ETZ 10a	TEQ 67	ETZ 3	TAL 11	TAL 25	TAL 7	TAL 13	TAL 12
	flow	flow	cone	flow	cone	flow	cone	flow	flow	cone	cone	cone
SiO_2	60.3	62.2	58.1	58.2	58.8	59.0	59.4	59.4	59.7	59.8	60.7	62.0
TiO_2	0.81	0.74	1.18	1.15	1.46	1.28	1.23	1.42	1.44	1.42	1.27	1.14
Al_2O_3	17.7	16.9	17.1	16.9	16.1	16.7	16.5	16.4	16.3	16.2	16.2	16.2
FeO[a]	5.37	4.51	6.61	6.51	7.24	6.04	6.42	6.40	6.32	6.51	6.16	5.19
MnO	0.10	0.08	0.12	0.11	0.12	0.11	0.11	0.12	0.12	0.12	0.11	0.11
MgO	3.11	2.29	3.11	3.05	2.78	3.11	3.00	2.54	2.40	2.44	2.51	2.50
CaO	6.05	4.95	6.14	6.12	5.81	6.11	6.01	5.38	5.19	5.32	5.39	5.25
Na_2O	4.06	3.25	4.18	3.99	4.28	4.12	4.20	4.16	4.13	4.49	4.37	4.28
K_2O	1.91	2.93	1.91	2.06	2.20	2.05	2.07	2.57	2.79	2.31	2.35	2.44
P_2O_5	0.27	0.19	0.31	0.32	0.38	0.39	0.43	0.49	0.52	0.52	0.41	0.36
LOI			0.43	0.77	–0.23	0.10	0.02	0.62	0.44	–0.01	–0.19	–0.01
Total	99.66	97.98	99.17	99.23	98.91	98.98	99.40	99.60	99.37	99.08	99.26	99.48
Zr	176	188	170	151	168	187	182	222	236	206	156	191
Ba	628	808	721	740	685	734	776	829	874	776	832	766
Age (±1σ)	66±20	58±10	691±26	683±32	444±140	312±32	339±35	224±11	354±15	not dated	372±18	454±32
plag ph	1.0	10.6	0.8	0.3	0.8	1.4	1.9	1.0	1.1	0.5	1.0	2.6
plag mph	7.8	1.9	4.3	6.5	2.2	3.1	1.3	4.5	0.6	9.4	1.9	3.2
opx ph	-	1.0	-	0.5	-	-	0.8	0.3	0.5	0.6	0.4	0.2
opx mph	0.4	1.3	-	-	-	0.3	0.1	-	0.1	0.1	0.2	0.8
cpx ph	-	0.5	0.2	-	-	-	0.2	-	0.1	-	0.7	0.6
cpx mph	0.1	0.2	0.3	0.3	0.3	0.3	1.0	0.5	-	0.4	-	1.2
ol ph	-	-	-	-	-	-	-	-	-	-	0.4	0.3
ol mph	-	-	-	-	-	-	-	-	-	-	-	-
hbd ph	-	-	-	-	-	-	-	-	0.7	-	1.3	-
hbe mph	-	0.1	-	-	-	-	-	0.9	0.5	0.7	0.4	trace
oxide	-	trace	1.0	0.7	-	0.4	-	0.5	0.6	0.6	0.2	-
xls	9.3	15.6	6.6	8.3	3.3	5.5	5.3	7.7	4.2	12.3	4.6	8.9
gmass	90.7	84.4	93.4	91.7	96.7	94.5	94.7	92.3	95.8	87.7	95.4	91.1

Notes: Same as Table 1a. [a] Note the large LOI on these samples. Analyses and modes for PW samples are from Wallace and Carmichael (1994)

nocrysts of sanidine+plagioclase, and TEQ29 also has sparse hornblende.

$^{40}Ar/^{39}Ar$ geochronology methods

The applicability of the $^{40}Ar/^{39}Ar$ dating technique to Pleistocene lavas, and comparisons with conventional K-Ar dating was first documented by Hall and York (1978, 1984) and later revisited by Lanphere (2000). Previous work by Hildreth and Lanphere (1994), Singer et al (1997), Druitt et al (1999) and Hildreth et al (2003) have demonstrated the success of both K-Ar and $^{40}Ar/^{39}Ar$ methods in dating large numbers of arc volcanic rocks younger than 1 Ma. In this study, our strategy was to date as many different lavas as possible with an accuracy and precision of at least ±50 kyrs; in most cases the results are far better. Forty-nine samples were dated by the $^{40}Ar/^{39}Ar$ laser ablation, step-heating method. All analyses were run at the University of Michigan, and the procedures closely followed those described in Hall and Farrell (1995), Conway et al (1997), and Frey et al (2004). Groundmass was dated owing to the lack of potassic minerals in most samples, except in two cases (TEQ9 and TEQ29) where hornblende was dated. Glass was dated successfully (good replications and inter-laboratory comparisons as discussed below) for the obsidian samples.

Samples were taken from the interiors of lava flows or the inner cores of dense volcanic bombs from scoria cones, and each sample was checked for alteration using a petrographic microscope. Hand samples were crushed using a jaw crusher and ceramic mortar and pestle, and 1–2 mm-sized grains of groundmass were hand-picked under a binocular microscope in order to exclude grains with phenocrysts and/or vesicles. Grains were washed ultrasonically with deionized water and were packaged in 99.5% aluminum foil. Fish Canyon Tuff-3 biotite, with a K-Ar age of 27.99±0.04 Ma (2σ error) as calibrated against MMhb-1 (Hall and Farrell 1995; Samson and Alexander 1987) was used as the standard. This age is in agreement with the reported age of 27.95±0.09 Ma by Renne et al (1998) and the average age of 27.95 Ma reported by Baksi et al (1996). One packet of standard for approximately every five packets of groundmass was arranged in quartz tubes that were evacuated and sealed. Samples were irradiated with fast neutrons for six hours at the Phoenix-Ford Nuclear Reactor at the University of Michigan. The measure of the neutron flux, *J*, was monitored at five different heights of the quartz tube; interpolated *J* values were applied to age calculations for individual sample positions.

Five grains of each irradiated sample (5–20 mg) were loaded into individual wells of a copper tray and degassed (by heating overnight at 150–200 °C) into the evacuated

Table 4 Whole-rock major element (wt%) and trace element (ppm) composition and modal analyses (%) of dated samples

	Dacites						Rhyolites						Flows >1 Ma			
	V. Tequila?	Older peripheral flows and cones around V. Tequila														
	TEQ 23[a]	TAL 8	TAL 9	ETZ 11	ETZ 4	TEQ 66	TEQ 29[a]	TEQ21a	TEQ 18	TEQ 22	TEQ 45b	TEQ 35	ETZ 7	ETZ 5	TEQ 9[a]	ETZ 2[a]
	pumice	cone	cone	cone	cone	flow	pumice	obsidian	obsidian	obsidian	obsidian	obsidian	obsidian	flow	tuff	flow
SiO_2	63.6	64.6	66.3	66.6	67.5	68.4	73.7	74.1	74.1	74.5	75.0	75.4	75.8	55.2	55.2	61.4
TiO_2	0.62	0.93	0.77	0.71	0.53	0.68	0.09	0.15	0.11	0.15	0.12	0.11	0.16	1.79	1.21	0.67
Al_2O_3	15.8	15.7	15.4	15.5	15.3	14.6	12.6	13.3	12.3	13.4	13.1	12.6	13.1	16.8	16.2	17.4
FeO[a]	3.33	4.27	3.95	3.55	3.10	3.07	1.21	1.46	1.35	1.32	1.32	1.34	1.15	8.65	5.69	4.72
MnO	0.06	0.09	0.08	0.09	0.10	0.07	0.05	0.06	0.05	0.04	0.06	0.06	0.04	0.14	0.13	0.07
MgO	1.10	1.33	1.56	0.94	0.50	0.92	0.05	0.11	0.08	0.13	0.07	0.06	0.17	2.44	2.40	2.07
CaO	3.47	3.46	3.55	2.57	1.48	2.33	0.48	0.51	0.42	0.63	0.42	0.39	0.86	5.82	5.48	5.89
Na_2O	3.19	4.75	4.48	5.06	5.47	4.44	3.69	4.61	4.35	4.50	4.67	4.45	4.20	4.62	2.79	4.00
K_2O	2.50	3.00	3.30	3.65	4.29	3.89	4.60	4.83	4.62	4.71	4.77	4.66	4.31	1.99	1.71	1.49
P_2O_5	0.16	0.32	0.23	0.22	0.13	0.22	0.02	0.03	0.02	0.03	0.02	0.02	0.04	0.58	0.37	0.19
LOI	6.04	0.28	0.02	0.16	0.52	−0.06	3.81	1.14	0.67	0.87	0.20	1.25	0.43	1.08	8.12	1.59
Total	99.80	98.71	99.70	99.10	98.84	98.59	100.33	100.33	98.07	100.26	99.80	100.31	100.24	99.06	99.33	99.50
Zr	189	249	259	404	811	237	163	263	234	183	254	228	157	251	207	129
Ba	930	913	927	957	1370	852	166	342	55	940	81	53	911	820	823	666
Age (±1σ)	not dated	374±11	404±15	619±8	635±4	383±4	1121±149	622±3	642±6	416±3	604±3	632±8				
plag ph	1.0	1.9	1.1	2.3	-	1.2	9.0	0.6	-	-	-	-				
plag mph	0.3	3.4	1.0	6.0	3.4	6.0	0.5	0.3	-	-	-	-				
opx ph	0.1	-	0.3	-	1.8	-	-	-	-	-	-	-				
opx mph	0.4	0.2	0.1	-	0.1	0.3	-	-	-	-	-	-				
cpx ph	-	0.7	0.1	-	0.1	0.5	0	-	-	-	-	-				
cpx mph	0.2	0.3	0.2	0.2	0.2	0.3	-	-	-	-	-	-				
hbd ph	-	1.2	-	1.3	-	-	0.1	-	-	-	-	-				
hbd mph	-	0.2	0.9	0.4	-	1.5	-	-	-	-	-	-				
alk fspar ph	1.2	-	0.2	-	-	-	3.9	1.2	-	-	-	-				
alk fspar mph	0.5	-	-	-	-	-	-	0.4	-	-	-	-				
quartz ph	-	-	0.2	-	-	-	-	-	-	-	-	-				
xls	3.7	7.9	4.1	10.2	5.6	9.8	13.5	2.5	0.0	0.0	0.0	0.0				
gmass	96.3	92.1	95.9	89.8	94.4	90.2	86.5	97.5	100.0	100.0	100.0	100.0				

Notes: Same as Table 1a. Abbreviations: alk fspar=alkali feldspar. [a] Note the large LOI on these samples

laser-line system to remove excess atmospheric argon. Samples were then step-heated at increasing levels of laser power from 100 to 4000 mW (13 steps for groundmass) using a defocused beam from a Coherent Innova 5-W continuous argon ion laser. The laser power was directed at individual sample grains for 30 s at each temperature while the gas was cleaned by a liquid nitrogen-chilled cold finger and two SAES ST101 alloy getters operating at 0.45 A. Peaks over the mass range 40–36 were measured on a Daly detector. Fusion system blanks were subtracted from gas fractions at the five Ar mass positions, and blank levels were monitored after every fifth sample fraction. The data were corrected for interference reactions due to Ca, K, and Cl and for ^{37}Ar and ^{39}Ar decay. Ages were calculated using the decay constants in Steiger and Jäger (1977). Mass discrimination was monitored daily with an atmospheric Ar gas pipette and had a precision of 0.3–0.5% for the $^{40}Ar/^{36}Ar$ ratio.

$^{40}Ar/^{39}Ar$ results and assessment of accuracy

The $^{40}Ar/^{39}Ar$ data analysis for each sample, including gas spectra and inverse isochron diagrams, as well as a complete degassing history are given in the Data Repository (Electronic Supplementary Material, ESM Fig. 1 and ESM Tables 1a–1d, 2, 3, 4). A summary of this information along with total gas, correlation, and plateau ages are reported for each sample in Table 5. The error analysis for each sample includes uncertainties in peak signals, system blanks, spectrometer mass discrimination, reactor corrections, and *J* values. The error on the plateau age is a standard weighted error for the individual steps by variance (Taylor 1982), so release fractions with more precise results carry greater weight in the age calculation. Seven samples $\leq$1 Ma had disturbed spectra that did not result in a plateau; correlation and total gas ages are presented in Table 6. For these samples, the isochron age is preferred because $^{40}Ar/^{36}Ar$ intercepts are within 2σ of 295.5 (atmosphere) in all cases but one. Four samples are >1 Ma and are reported separately in Table 7.

The accuracies of the $^{40}Ar/^{39}Ar$ dates reported in Tables 5, 6, and 7 were evaluated in three different ways: (1) a comparison with stratigraphic relations observed in the field, (2) a comparison with dates obtained on the same samples, but from other laboratories (Table 8), and (3) a replication of dates obtained in this study. Errors throughout the paper are given at the 1σ level except where stated otherwise.

Stratigraphic relations

The $^{40}Ar/^{39}Ar$ geochronology is supported in all cases where a stratigraphic relation is observed in the field. We have documented eleven examples. (1) In the town of Santa Teresa, the basalt flow fed from scoria cone TEQ36 (261±11 ka) overlies the rhyolite flow of TEQ45b (604±3 ka). (2) The same basalt flow (TEQ36, 261±11 ka) overlies the capping basalt flow near the rim of the Rio Grande de Santiago Canyon (dated at 848±20 ka by Wopat 1990); it flowed around and about the dacite flow of San Martin (dated at 630±30 ka by Nixon et al 1987). (3) The basaltic andesite flow from scoria cone TEQ37 (427±20 ka) overlies the rhyolitic dome and flows of TEQ18/TEQ35 (642±6 ka; 632±8 ka). (4) Flows from Cerro Tomasillo, which have a mean age of 62±11 ka, overlie flows that form the main edifice of Volcán Tequila, which have a mean age of 196±12 ka. (5) Lavas from Cerro Tomasillo (62±11 ka) flowed around the dacite domes immediately to the SE. Nixon et al (1987) report that these dacite domes are overlain by Tala Tuff airfall deposits (95±10 ka; Mahood 1981); they are therefore older than 75 ka at the 2σ level. (6) A lobe from the main edifice of V. Tequila (196±12 ka) and a lobe from Cerro Tomasillo (62±11 ka) each flowed around either side of scoria cone TAL13 (372±18 ka). (7) The northernmost lobe of V. Tequila (TEQ60; 178±8 ka) overlies the rhyolitic dome TEQ22 (416±3 ka). (8) The basalt flow TEQ10 (671±13 ka) from the southern wall of the Rio Grande de Santiago Canyon is underneath basalt flow TEQ12 (592±20 ka). (9) The basaltic andesite flow TEQ40 (194±15 ka) flowed around and about the basaltic scoria cone TEQ39 (970±34 ka). (10) The andesite flank flow of TEQ46/TEQ48 (mean age of 86±47 ka) flowed around the basaltic andesite scoria cone TEQ33 (362±13 ka). (11) The andesite flow of PW123 (87±12 ka) overlies the W flank of V. Tequila (196±12 ka).

Interlaboratory comparisons

Our $^{40}Ar/^{39}Ar$ results are in excellent agreement with previously published ages in all cases where the same lava flows or samples were dated. Table 8 compares the results of our age analyses with K-Ar dates from the Berkeley Geochronology laboratory in 1985, 1986, and 1990 as well as with an unidentified laboratory (Nixon et al 1987). All of the dates being compared are within 2σ error except one; the exception comes within 16 kyrs of overlapping error on a date of 420–450 kyrs (Table 8). Sample locations may be found using Figs. 2 and 3 in conjunction with Table 8.

Replications

As a check on our $^{40}Ar/^{39}Ar$ method, different samples from the same volcanic edifice/flow were dated in order to evaluate the consistency between results. (1) Six samples were taken from different parts of the main edifice of V. Tequila (TEQ15, TEQ23C, TEQ60, TEQ17, TEQ6, 1075-Q9a; Fig. 2) and resulted in a series of dates (196±8, 196±19, 178±8, 191±13, 216±11, and 198±11 ka) that are all within 2σ error of each other. The mean eruption age for the main edifice of V. Tequila is therefore 196±12 ka. These results further suggest, within a

Table 5 $^{40}Ar/^{39}Ar$ total fusion, isochron, and plateau ages ≤1 Ma, Tequila volcanic field. Arranged oldest to youngest

Sample #	Lava Type	Coordinates	Total Gas Age (ka)	Correlation Age (ka)	Correlation MSWD	Points fitted	$(^{40}Ar/^{36}Ar)_i$	Plateau Age (ka)	Plateau MSWD	Plateau % ^{39}Ar
TEQ 29	rhyolite	20°54.80 103°58.50	978±283	1137±152	0.44	17 of 17	295±2	1121±149[a]	0.43	100
TEQ 31	andesite-p	20°47.68 103°42.43	617±20	768±31	0.83	9 of 14	289±2	691±26[a]	1.89	85
TEQ 38	andesite-p	20°50.30 103°43.50	616±29	524±73	0.68	9 of 13	301±2	683±32[a]	1.30	70
TEQ 10	basalt	20°53.88 103°44.18	700±21	668±13	1.79	13 of 13	299±3	671±13[a]	1.99	89
TEQ 18	rhyolite	20°53.42 103°56.60	634±8	643±7	1.67	13 of 13	282±13	642±6[a]	0.37	96
TEQ 35	rhyolite	20°51.81 103°58.65	612±12	632±11	0.85	7 of 13	294±23	632±8[a]	0.71	97
ETZ 4	dacite	20°48.35 104°01.43	642±6	635±5	1.64	13 of 13	296±2	635±4[a]	0.87	93
TEQ 21a	rhyolite	20°51.26 103°51.86	615±5	620±4	2.23	13 of 13	301±31	622±3[a]	0.67	84
ETZ 11	dacite	20°47.00 103°00.46	624±10	646±31	0.46	13 of 13	289±8	619±8[a]	0.48	100
TEQ 45b	rhyolite	20°54.76 103°53.44	603±6	603±4	0.54	13 of 13	296±1	604±3[a]	0.51	100
TEQ 12	basalt	20°53.99 103°43.71	631±27	595±26	0.32	8 of 13	294±7	592±20[a]	0.28	88
TAL 12	andesite-p	20°41.98 103°47.78	458±36	499±32	0.65	8 of 13	282±6	454±32[a]	1.38	93
TEQ 37	BA	20°51.60 103°55.25	429±25	363±39	0.75	13 of 13	299±2	427±20[a]	1.00	100
TEQ 22	rhyolite	20°50.46 103°49.66	420±7	414±5	0.97	13 of 13	356±124	416±3[a]	1.10	85
TAL 9	dacite	20°44.91 103°55.24	375±24	393±24	2.52	13 of 13	299±3	404±15[a]	0.90	88
TEQ 66	dacite	20°48.15 103°59.02	378±7	384±3	0.55	13 of 13	261±20	383±4[a]	0.69	100
TAL 8	dacite	20°44.85 103°55.82	339±14	381±7	0.96	13 of 13	235±21	374±11[a]	1.94	94
TAL 13	andesite-p	20°44.70 103°49.50	354±36	356±28	0.48	5 of 13	305±13	372±18[a]	0.50	88
TEQ 33	andesite-p	20°49.75 103°59.69	371±14	320±59	0.95	13 of 13	300±6	362±13[a]	0.92	100
TAL 25	andesite-p	20°41.34 103°55.06	394±13	346±16	2.06	13 of 13	302±3	354±15[a]	2.28	81
ETZ 3	andesite-p	20°46.50 103°00.30	351±45	367±60	1.06	13 of 13	294±3	339±35[a]	0.86	86
TEQ 36	basalt	20°53.03 103°53.96	261±11	268±18	1.42	13 of 13	292±5	261±11[a]	1.33	100
TAL 11	andesite-p	20°40.79 103°56.05	271±19	287±10	1.01	5 of 13	292±5	224±19[a]	0.86	67
TEQ 6	andesite-m	20°47.38 103°50.96	227±16	210±14	1.01	13 of 13	312±19	216±11[a]	0.71	92
JH009[c]	andesite-m	20°47.27 103°50.57	211±12	185±16	0.57	13 of 13	322±18	198±11[a]	0.64	98
TEQ 23c	andesite-m	20°50.02 103°48.79	211±11	190±22	5.52	13 of 13	299±8	196±19[a]	5.13	96
TEQ 15	andesite-m	20°47.41 103°51.08	223±9	189±17	2.93	6 of 13	312±28	196±8[a]	2.56	87
TEQ 40	BA	20°50.70 103°46.10	233±18	214±17	0.96	5 of 13	291±2	194±15[a]	1.36	77
TEQ 17	andesite-m	20°48.60 103°50.70	162±16	221±20	0.92	9 of 13	286±3	191±13[a]	0.47	61
TEQ 60	andesite-m	20°51.96 103°50.42	187±11	176±13	0.91	10 of 13	298±14	178±8[a]	0.82	97
TEQ 25	andesite-m	20°49.26 103°47.79	167±15	162±20[a]	2.38	13 of 13	291±6	150±18	2.47	95
ETZ 1	basalt	20°49.60 104°05.00	145±15	147 38	0.51	13 of 13	293±13	140±12[a]	0.47	100
TEQ 48	andesite-f	20°49.15 103°58.43	135±18	108±27[a]	1.59	13 of 13	296±1	119±18	1.51	100
TEQ 46	andesite-f	20°50.06 103°58.81	56±20	73±24[a]	0.71	13 of 13	293±3	53±16	0.75	100
TAL 1	andesite-f	20°41.32 103°41.83	55±11	93±11	1.75	13 of 13	284±9	87±11[a]	1.83	100
PW123[b]	andesite-f	20°47.59 103°53.11	96±16	82±14	0.54	13 of 13	299±4	87±12[a]	0.44	99
PW391[b]	andesite-f	20°45.51 103°47.77	85±27	51±37	0.81	13 of 13	297±3	66±20[a]	0.39	69
PW143[b]	andesite-f	20°45.32 103°46.71	85±13	53±16	1.80	7 of 13	298±7	58±10[a]	1.56	86

Lava types: andesite-p (peripheral to V. Tequila), andesite-m (main edifice of V. Tequila), andesite-f (younger flanks of V. Tequila), BA (basaltic andesite). All errors are ±1σ. [a] Preferred age; [b] collected by Wallace and Carmichael (1994); [c] collected by Harris (1986). All correlation diagrams with MSWD>1.8 are considered errorchrons. Plateau ages are error weighed averages with scatter included in the error estimate. Groundmass was dated in all samples except for TEQ29 for which hornblende was used

Table 6 $^{40}Ar/^{39}Ar$ total fusion and isochron ages, Tequila volcanic field

Sample #	Coordinates	Total Gas Age (ka)	Correlation Age (ka)	Points fitted	$(^{40}Ar/^{36}Ar)_i$	Volume (km^3)
ETZ 6	20°49.60 104°02.60	956±48[a]	1130±159	6 of 13	293±3	individual flow
TEQ 39	20°50.85 103°45.45	970±34	985±68[a]	13 of 13	294±2	0.01
TEQ 32	20°46.23 103°40.52	960±42	662±60[a]	13 of 13	297±1	0.08
ETZ 10	20°45.40 104°00.70	124±134	444±140[a]	13 of 13	295±1	0.07
TAL 26	20°41.10 103°52.79	248±15	343±38[a]	13 of 13	288±3	0.03
TEQ 67	20°48.16 103°58.94	626±110	312±32[a]	13 of 13	297±1	1.3
PW 133[b]	20°49.57 103°56.87	95±42[a]	114±79	8 of 13	293±2	individual flow

All errors are ±1σ. [a] Preferred age; [b] collected by Wallace and Carmichael (1994). Correlation diagrams with MSWD>1.8 are considered errorchrons. Plateau ages are error weighed averages with scatter included in the error estimate. Groundmass was dated in all samples

95% confidence interval, that the bulk of the main edifice was erupted within ≤24 kyrs. (2) Two samples from Cerro Tomasillo (PW139 and PW143), collected and described by Wallace and Carmichael (1994), resulted in ages of 66±20 and 58±10 ka, respectively. Although Wallace and Carmichael (1994) label sample 143 as a flank andesite and do not assign it to Cerro Tomasillo, its location (field map of Paul Wallace, personal communication, 2003) is clearly a flow from Cerro Tomasillo as revealed by the newly available aerial photographs and digital elevation models with 2 m vertical resolution (Fig. 2). (3) Two peripheral andesite samples of nearly identical composition (Tables 1a–1d, 2, 3, 4) taken from a cinder cone (TEQ31) and the distal edge of its associated lava flow (TEQ38) were both dated and gave nearly identical results (691±26 and 683±32 ka, respectively). (4) Two rhyolite samples taken from the same dome (TEQ18 and TEQ35) with nearly identical major and trace element compositions also gave indistinguishable results (642±6 ka, 632±8 ka). (5) Two andesite samples

Table 7 $^{40}Ar/^{39}Ar$ total fusion, isochron, and plateau ages >1 Ma, Tequila volcanic field

Sample #	Coordinates	Total Gas Age (ka)	Correlation Age (ka)	Correlation MSWD	Points fitted	$(^{40}Ar/^{36}Ar)_i$	Plateau Age (ka)	Plateau MSWD	Plateau % ^{39}Ar
TEQ 9	20° 54.60 103°43.20	5118±62	5120±51	0.57	17 of 17	300±9	5137±47[a]	0.45	96
ETZ 5	20°49.89 104°02.12	3911±37	3891±35[a]	3.06	13 of 13	295±3	-	-	-
ETZ 7	20°46.97 104°05.66	2905±12[a]	3058±45	3.89	15 of 15	282±4	-	-	-
ETZ 2	20°46.20 104°10.50	2306±34	2235±22	1.30	13 of 13	297±1	2238±24[a]	1.52	86

All errors are ±1σ. [a] Preferred age. All correlation diagrams with MSWD>1.8 are considered errorchrons. Plateau ages are error weighed averages with scatter included in the error estimate. Groundmass was dated in all samples except for TEQ9 for which hornblende was used

Table 8 Interlaboratory comparison of age determinations from the Tequila volcanic field

Volcanic feature	Sample # (this study)	$^{40}Ar/^{39}Ar$ age ±2σ (this study)	K-Ar age ±2σ (literature)	References from literature
Rhyolite dome	TEQ 22	416±06	456±18	JH46; Harris (1986)[a]
Rhyolite dome	TEQ 35	632±16	614±20	JH142; Harris (1986)[a]
Santa Rosa plateau	TEQ 12	592±40	528±75	995–033; Gilbert et al (1985)[a]
Santa Rosa plateau	TEQ 12	592±40	524±36	1081–011; Wopat (1990)[a]
Spine of V. Tequila	JH009	198±22	206±14	JH009; Harris (1986)[a]
Summit of V. Tequila	TEQ 6	216±22	220±30	GN506; Nixon et al (1987)[b]

[a] Age obtained from Berkeley Geochronology Center; [b] Laboratory that provided the age is not identified. The same specimen, JH009, was dated in this study and in Harris (1986). A sample close to TEQ12 was sampled and dated by Nixon et al 1987 at 930 ka; it may mark the boundary between a younger basalt lapping against an erosional remnant of an earlier sequence

from the same NW flank flow (TEQ46/TEQ48) with nearly identical compositions (Tables 1a–1d, 2, 3, 4) gave the same age within error. Their preferred isochron ages are within 1σ of each other (73±24 ka and 108±27 ka), with a mean age of 91±25 ka. These flank andesite lavas were among the most difficult to date owing to their youthfulness and vesicularity.

Summary of results for samples ≤1 Ma

A plot of age versus silica content for the Tequila volcanic field is shown in Fig. 4, which includes data from this study and from the literature. There is no pattern of increasing silica content with time over the last 1 Myr. The preferred ages for each lava type (basalt, basaltic andesite, andesite, dacite, rhyolite) are also given in Tables 1a–1d, 2, 3, 4. The earliest eruptions of basalt occurred between 1 and 0.85 Ma ago within the Rio Grande de Santiago Canyon; the geographic distribution of ages, morphology of flows, and petrographic textures strongly suggest that this episode of basaltic volcanism led to complete filling, ponding, and overflowing of this segment of the canyon, creating the primary surface of the Santa Rosa Plateau. Flows that clearly post-date this primary surface include the TEQ31/TEQ38 andesite cone and flow near the town of Amatitan (691±26; 683±32 ka) and the 630 ka dacite flow, north of the town of Tequila, dated by Nixon et al (1987). One of the rhyolite domes (JH260, Fig. 2), with an age of 675±20 ka, is partially covered by the Santa Rosa Plateau basalt along its SW

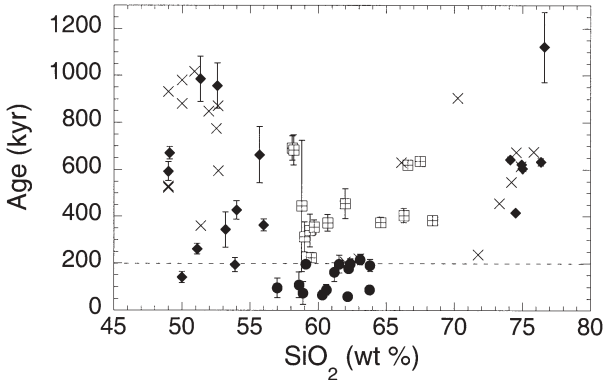

Fig. 4 The age (and 2σ error) of each dated eruptive unit ≤1 Myr in the Tequila volcanic field as a function of silica concentration; there is no correlation. The basalts, basaltic andesites, and rhyolites from this study are solid triangles. The andesites from the main edifice and flanks of V. Tequila are solid dots. The peripheral, small-volume andesites and dacites are crosses enclosed by squares. For comparison, dates from the literature (Damon et al 1979; Nieto-Obregón et al 1985, Nixon et al 1987; Gilbert et al 1985; Harris 1986; Wopat 1990) are also shown (× marks) without error bars

quadrant. Harris (1986) interpreted this as evidence of an eruption of basalt through the rhyolite dome. However, a more likely scenario is that this rhyolite dome intruded beneath the older basalt plateau and uplifted a portion of the basalt (Figs. 2 and 3). Similar relationships of rhyolite domes intruding and uplifting portions of older basalt flows are well documented in the Quaternary volcanic fields of the Snake River Plain (Hughes et al 1999).

Basaltic eruptions continued to occur within the canyon; the next series of eruptions occurred between ~670 and 590 kyrs ago (TEQ10 and TEQ12) and appear to have filled the canyon locally and possibly caused the river to be re-routed hundreds of meters northward. The most recent eruption of basalt within the canyon produced a lava cone dated by Wopat (1990) at 364±46 ka (MW-72, Fig. 3). Between 0.95 and 0.19 Ma, at least six different basalt and basaltic andesite eruptions occurred from isolated vents located on top of the Santa Rosa Plateau. The youngest dated basalt (140±12 ka) is from scoria cone ETZ1, which is west of V. Tequila (Figs. 2 and 3).

The first eruptions of andesite were all peripheral to V. Tequila and include both scoria cones and small lava flows. The oldest andesite (within the last 1 Myr) erupted ~690 kyrs ago as a scoria cone and associated flow on top of the Santa Rosa Plateau (TEQ31/38). The next andesite eruptions all occurred west and south of V. Tequila as small flows and scoria cones between ~450 and ~225 kyrs ago. The main edifice of V. Tequila is predominantly andesitic and appears to have erupted over a relatively narrow time interval ($\leq$24 kyrs) at ~200 ka. After an apparent hiatus of ~110 kyrs, young andesite flows erupted at ~90 ka along the W (PW123, PW133, TEQ46, TEQ48) and SE (TAL1) flanks of V. Tequila. The youngest eruption of andesite (and the youngest feature in the Tequila volcanic field) built Cerro Tomasillo at ~60 ka.

Two andesite samples from one of the flank flows SE of V. Tequila (TAL21 and TAL27) of nearly identical bulk composition (Tables 1a–1d, 2, 3, 4) yielded highly disturbed gas spectra without a plateau. The age of the flow, however, is bracketed between ~200 and ~75 ka based on stratigraphic relations. Along its western margin, the lava flowed on top of the southernmost flows from V. Tequila (196±12 ka) as well as around the W and SE sides of scoria cone TAL12 (454±32 ka). The flow is overlain by both Cerro Tomasillo (62±11 ka) and the dacite domes and associated flows (>75 ka). Its eruption may have been broadly contemporaneous with the other andesite flank eruptions W and SE of V. Tequila, all of which have $^{40}Ar/^{39}Ar$ dates that cluster ~90 kyrs ago.

Dacite first erupted at ~630 ka as a series of scoria cones west of V. Tequila (ETZ4, ETZ11) and also as a flow on top of the Santa Rosa Plateau (north of the town of Tequila; dated by Nixon et al 1987). The next dacite eruptions were two small scoria cones southwest of V. Tequila at ~390 ka (TAL8, TAL9). Small remnants of a dacitic airfall deposit (TEQ23) are found underneath a small block and ash deposit of two-pyroxene andesite (TEQ23c), which has been dated at 196±19 ka. Therefore, it appears that a small explosive eruption of dacite from the main edifice of V. Tequila occurred ~200 kyrs ago. The youngest dacite (erupted sometime between 200 and 75 kyrs ago) occurs as a series of small domes and associated flows that are immediately SE of Cerro Tomasillo.

Rhyolitic flows have erupted sporadically between 1120 and 240 kyrs ago throughout the field area (on all sides of V. Tequila) with the greatest frequency of eruption between 400 and 700 kyrs ago. No rhyolite has erupted since the onset of major andesitic volcanism at ~200 ka, when the main edifice of V. Tequila was built.

Samples >1 Ma

Four dated samples are older than 1 Myr (Table 7) and are not included in the inventory of erupted volumes. The oldest (TEQ9, 5.14±0.05 Ma) is a hornblende-bearing andesitic ash-flow tuff that erupted onto (and was covered by) lake sediments and is located on the southern wall of the Rio Grande de Santiago Canyon stratigraphically beneath TEQ10, in view of the Santa Rosa dam. This is likely the same unit that was dated by Damon et al (1979) at 4.69 Ma and described as a hornblende tuff. The other three are samples from west of V. Tequila and are all crystal-poor to aphyric. One is an andesite (ETZ2, 2.24±0.02 Ma) and lies outside the field area, whereas the other two are a basaltic andesite and a rhyolite, respectively, in the western part of the field area (ETZ5, 3.86±0.04 Ma and ETZ7, 3.02±0.05 Ma; Figs. 2 and 3).

Volumes

Methods and errors

The total volume of magma erupted at the Tequila volcanic field over the last 1 Myr was determined from our geologic field map combined with analysis of ortho aerial photographs (1:20,000) and DEMs (1:50,000) using the GIS software ArcView 3.2 and ArcGIS 8.1 (Table 9). The Universal Transverse Mercator (UTM) projection and the Geodetic Reference System 80 (GRS 80) model is used for both, allowing the DEMs to be superimposed on the airphotos. The DEMs have a vertical resolution of 2 m. In order to evaluate the volumes of volcanic cones, domes, and flows, a three-dimensional surface of the geologic map was created with ArcGIS software (for details of the procedure and error analysis, see Frey et al 2004).

The most challenging aspect of the volume calculations was determining the slope, elevation, and topography of the basal surface beneath each unit. Errors are smallest for units with well-exposed boundaries, including scoria cones and isolated domes and flows. Large errors in volume occur where andesitic or rhyolitic flows or domes are ponded against older units or if overlying flows obscure the thickness of the units at the perimeter. To estimate the thickness of a ponded flow, the underlying slope was calculated where it was visible and extended to the contact so that the elevation at the base of the flow could be estimated. Where a flow was partially buried, the thickness around the exposed edge was measured and the concealed thickness estimated. This procedure was checked by estimating the thickness of the flow from the elevation of the underlying surface. It resulted in large errors in the case of scoria cones where

Table 9 Volumes of all eruptive units ≤1 Ma at the Tequila volcanic field

Lava Type	Eruptive unit	Volume (km^3)	% Error	Minimum Volume (km^3)	Maximum Volume (km^3)	% of Total
Andesite	Cerro Tomasillo	1.9±0.2	11	1.70	2.10	
	ETZ3	0.040±0.002	5	0.038	0.042	
	ETZ10	0.070±0.004	6	0.066	0.074	
	Young W flank	8±2	25	6	10	
	TAL7	0.080±0.004	5	0.076	0.084	
	TAL12	0.02±0.01	50	0.01	0.03	
	TAL13	0.02±0.01	50	0.01	0.03	
	Young SE flank	7.0±1.7	26	5.2	8.8	
	TAL25	0.41±0.03	7	0.38	0.44	
	TEQ31/38	0.20±0.02	10	0.18	0.22	
	TEQ52	0.3±0.1	33	0.2	0.4	
	TEQ67	1.3±0.4	31	0.9	1.7	
	V. Tequila	31±2	7	28.9	33.1	
	Subtotal	50.3±6.6	13	43.8	56.8	29–54
Basaltic andesite	TAL26	0.03±0.01	33	0.02	0.04	
	TEQ32	0.080±0.024	30	0.056	0.104	
	TEQ33	0.010±0.001	10	0.009	0.011	
	TEQ37 flow	0.47±0.20	43	0.27	0.67	
	TEQ37 cone	0.010±0.001	10	0.009	0.011	
	TEQ40	0.2±0.01	5	0.199	0.201	
	Subtotal	0.80±0.24	31	0.56	1.04	0.4–1.0
Basalt	ETZ1	0.030±0.002	7	0.028	0.032	
	TAL3	0.010±0.001	10	0.009	0.011	
	TEQ36	0.010±0.001	10	0.009	0.011	
	TEQ36 flow	0.6±0.2	33	0.4	0.80	
	TEQ39	0.010±0.001	10	0.009	0.011	
	Canyon fill ~1 Ma	24±2	8	22	26	
	Santa Rosa plateau	9±3	33	6	12	
	Canyon fill ~670 ka	4.4±1	23	3.4	5.4	
	Canyon fill ~590 ka	0.83±0.40	48	0.43	1.23	
	Subtotal	38.9±6.6	17	32.29	45.49	22–43
Dacite	SE of C. Tomasillo	1.10±0.05	5	1.05	1.15	
	ETZ4	0.040±0.004	10	0.036	0.044	
	ETZ11	0.10±0.01	10	0.090	0.110	
	GN624	1.20±0.14	12	1.06	1.34	
	GN624a	0.150±0.015	10	0.14	0.17	
	GN626b	0.090±0.008	9	0.08	0.10	
	TAL8	0.040±0.004	10	0.036	0.044	
	TAL9	0.04±0.02	50	0.020	0.060	
	TAL17	0.21±0.05	24	0.16	0.26	
	Subtotal	3.0±0.3	10	2.7	3.3	1.8–3.1
Rhyolite	NE of TEQ25	0.15±0.05	33	0.10	0.20	
	JH147	0.57±0.06	11	0.51	0.63	
	JH182	1.00±0.25	25	0.75	1.25	
	JH201	2.5±0.5	20	2.0	3.0	
	JH257	3±1	33	2	4	
	JH260	1.9±0.5	26	1.4	2.4	
	W of JH147	0.22±0.01	5	0.21	0.23	
	TEQ21	16±4	25	12	20	
	TEQ22	2.1±0.2	10	1.9	2.3	
	TEQ29	1.20±0.06	5	1.14	1.26	
	W of TEQ33	0.10±0.01	10	0.09	0.11	
	S of TEQ33	0.37±0.08	22	0.29	0.45	
	TEQ35	4.7±1.0	21	3.7	5.7	
	TEQ45	1.00±0.25	25	0.75	1.25	
	Subtotal	34.8±8.0	23	26.8	42.8	18–40
Total		128±22	17	106	150	

the younger flow was thick enough to cover a significant part of the volume of the cone. Overall, these large errors do not affect rate calculations because the volumes of the cones are so small. Maximum and minimum volumes were estimated by varying the thickness of the flow and the elevation (degree of slope) of the underlying surface.

The most complex areas for volumetric calculations occur where rhyolitic domes and flows are partially covered by younger andesitic flows, on the west side of Volcán Tequila. In these cases, the minimum volume is based on the area of the exposed dome and a horizontal base level at the lowest point of the perimeter. The sides were assumed to be vertical, which is consistent with their

steep margins observed in the field. The maximum volume is calculated by assuming that the exposed area is a fraction of an idealized, circular dome where the highest elevation of the exposed dome is assumed to be the center. The volumes of the younger andesite flows that partially cover rhyolite flows and flank V. Tequila were calculated using their well-defined perimeters and an estimate of their thicknesses from the elevation and topography inferred for the underlying volcanic units. Minimum volumes were calculated by assuming that the flows had constant thicknesses over the exposed area.

Results

The results of the volume calculations are given in Table 9 in conjunction with sample identifications in Fig. 2. A relatively large volume is calculated for basalt owing to our interpretation that basalt filled the Rio Grande de Santiago Canyon ~1.0–0.9 Ma and subsequently flooded the Santa Rosa Plateau at ~0.85–0.9 Ma. The volume of canyon-fill up to 20–40 m below the southern rim (~1060–1080 m) is readily calculated and leads to a value of ~22–26 km^3. This volume is likely a maximum, as the canyon was probably less deeply incised at 1 Ma than today. On the other hand, this calculation does not account for the volume of basalt that filled the canyon downstream, north of our defined field area. The volume of basalt that is estimated to have covered the Santa Rosa Plateau at ~0.9–0.85 Ma relies on an estimate of the areal extent (~300 km^2), which is the sum of the currently exposed area (190 km^2) plus the area of the canyon at the 1100 m contour line (110 km^2). The thickness (~30 m) is based on that for the package of three flows described and dated (top and third flow) by Wopat (1990) that cap the canyon rim (MW77, MW78; Fig. 2). Thickness variations of 20–40 m led to minimum and maximum volumes for the plateau lavas of 6 and 12 km^3, respectively.

The sequence of dates obtained for TEQ12 (surface flow, 590 ka) and TEQ10 (ponded flow beneath TEQ12, 670 ka) suggest that a second infilling of the canyon occurred locally in this area. A total volume of 3–5 km^3 is estimated for this canyon-fill. The volumes of isolated basalt and basaltic andesite flows located on top of the Santa Rosa Plateau are 0.47±0.2 km^3 (TEQ37), 0.60±0.2 km^3 (TEQ36), and 0.20±0.01 km^3 (TEQ40), whereas individual scoria cones associated with the basalt flows are $\leq$0.01 km^3.

The main andesitic edifice, Volcán Tequila, has an estimated volume of 31±2.1 km^3, whereas the much smaller Cerro Tomasillo has a volume of 1.9±0.2 km^3. The western, younger andesitic flows that flank V. Tequila have a collective volume of 8±2 km^3, whereas the SE flank andesitic lavas have an estimated volume of 7±2 km^3. Peripheral andesitic flows and cones have a combined volume of 2.4±0.6 km^3. The dacite flow north of V. Tequila has a volume of 1.4±0.16 km^3, whereas the line of dacitic domes and associated flows SE of Cerro Tomasillo are 1.1±0.05 km^3. The peripheral dacitic scoria cones have a combined volume <0.19±0.005 km^3. The volume of the dacitic airfall deposit (TEQ23) is unknown due to extremely limited exposure and it is not included in our volume inventory. The 12 rhyolitic domes and flows have a total volume of 34.8±8.0 km^3. The largest dome/flow complex (TEQ21) is 16±4 km^3, whereas all other rhyolite domes and flows are significantly smaller (<5 km^3).

Total erupted volumes, relative proportions of lava types, and eruption rates

The total volume of each lava type erupted in the Tequila volcanic field over the last 1 Myr is 32–45 km^3 basalt, 0.6–1.0 km^3 basaltic andesite, 44–57 km^3 andesite, 2.7–3.3 km^3 dacite, and 27–43 km^3 rhyolite (Table 9). Therefore, the total erupted volume is 106–149 km^3 over an area of ~1600 km^2 in the last 1 Myr, which leads to an average eruption rate of 79 $m^3/km^2/yr$. This is equivalent to a lava accumulation rate averaged over the entire field area of ~79 m/Myr or ~8 cm/ky. The relative proportions of magmatic compositions erupted in the Tequila volcanic field in the last 1 Myr are 22–43% basalt, 0.4–1.0% basaltic andesite, 29–54% andesite, 2–3% dacite and 18–40% rhyolite.

A combination of the $^{40}Ar/^{39}Ar$ dates with the volume estimates for individual eruptive units allows a graphical representation of how the volumes of the different compositions were erupted over time (Fig. 5). The field exhibits a general trend of bimodal basalt-rhyolite volcanism between ~1.0 and 0.2 Myr ago, with only minor "background eruptions" of andesite and dacite occuring over this interval (Fig. 5). At ~200 ka, a pulse of volcanism produced ~31 km^3 of andesite to create Volcán Tequila, followed by a hiatus of ~110 ka, whereupon ~15 km^3 of flank andesite lavas were erupted. The eruption of ~1 km^3 of dacite followed soon after, and the last eruptive activity occurred at ~60 ka to produce ~2 km^3 of andesite in the form of Cerro Tomasillo.

The most recent and voluminous eruptions of andesite, including Volcán Tequila, its flank flows, and Cerro Tomasillo, all occurred within the last 200 kyrs, making the volcanism over this time period overwhelmingly andesitic (~97%). The relative proportions of lava types is very different if only the first 800 kyrs of the last 1 Myr is considered. Over that time interval, the proportions are ~53% basalt, ~1% basaltic andesite, ~2.5% andesite, ~2% dacite and ~41% rhyolite. Therefore, for a meaningful evaluation of eruption rates at an arc volcanic field, it is necessary to define the timescale of interest, as also emphasized by Hildreth et al (2003). This point is illustrated by comparing the eruptive history of the Tequila volcanic field with that documented for the Ceboruco-San Pedro volcanic field (~75 km northwest of Tequila) over the last 1 Myr (Frey et al 2004) (Fig. 5).

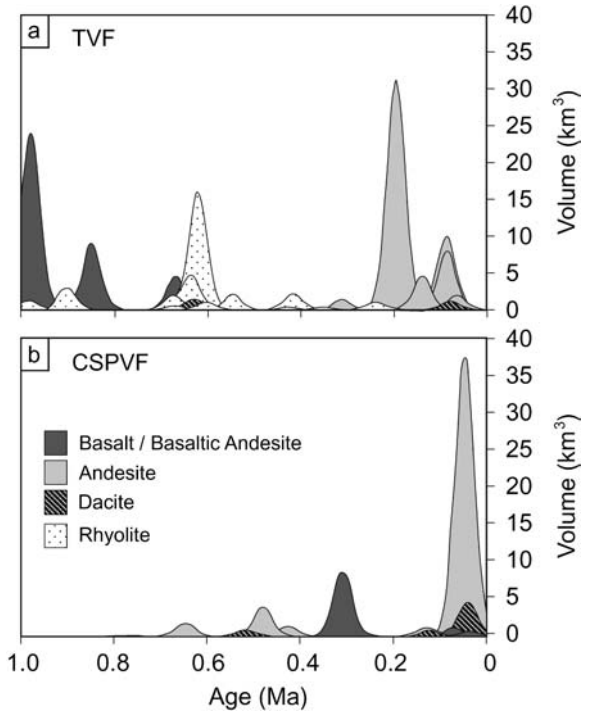

Fig. 5 Schematic diagrams of relative volumes of **a** lavas erupted $\leq$1 Ma in the Tequila volanic field (TVF) and **b** the relative volumes of lavas erupted $\leq$1 Ma in the Ceboruco-San Pedro volcanic field (CSPVF) (Frey et al 2004). The apex of each peak represents the average $^{40}Ar/^{39}Ar$ age (*x*-axis) and the volume of erupted units (*y*-axis). The width of each distribution curve represents a uniform, average error of ±40 kyrs. By assigning an equal error, both the height and area under each curve represent the relative volumes of each volcanic unit

Comparison with the Ceboruco-San Pedro volcanic field

The relative proportions of magmatic compositions erupted in the Ceboruco-San Pedro volcanic field in the last 1 Myr are 0% basalt, ~14–15% basaltic andesite, ~62–66% andesite, ~18–22% dacite, and ~1% rhyolite (Frey et al 2004). The distribution of the erupted volumes of these lava types over time is shown in Fig. 5 and compared to that for the Tequila volcanic field. The most striking difference is the paucity of basalt and rhyolite in the Ceboruco-San Pedro volcanic field and their relative abundance in the Tequila volcanic field between 1 and 0.2 Myr ago. In contrast, andesite and dacite constitute the peripheral (non-central) volcanism at the Ceboruco-San Pedro volcanic field over this time period. Another difference is in the total output of erupted magma over the entire 1 Myr interval in each volcanic field, ~81±4 km^3 versus ~128±22 km^3, over similar areas (1600 km^2). Therefore, the lava accumulation rate (volume per area) differs between the two volcanic fields by more than 40% (~5 versus ~8 cm/kyr) over the last 1 Myr.

The most striking similarity between the two volcanic fields is the voluminous intermediate (andesite/dacite) volcanism in the last few hundred kyrs. The relative proportions of magma types erupted in the last 200 kyrs at the Ceboruco-San Pedro volcanic field are ~4% basaltic andesite, ~71% andesite, ~23% dacite, and ~2% rhyolite, and at the Tequila volcanic field are ~97% andesite and ~3% dacite. Another similarity is that both volcanic fields record a hiatus in volcanism between the mid-Pliocene and ~1 Ma. Frey et al (2004) document a hiatus in the Ceboruco-San Pedro volcanic field between 3.8 and 0.8 Ma. At the Tequila volcanic field, with the single exception of a small andesite flow outside the field area (ETZ2, 2 Ma), there appears to be a hiatus between ~3 and 1 Ma. Lavas that cap the northern rim of the Rio Grande de Santiago Canyon north of Tequila have been dated at 3.7 and 3.9 Ma (Damon et al 1979) and we report ages of 3.0 and 3.9 Ma on a rhyolite and basaltic andesite, respectively, west of V. Tequila. These are the youngest lavas prior to the eruption of the basaltic Santa Rosa Plateau and the first of the rhyolite flows at ~1 Ma. This hiatus in volcanism coincides with the temporary cessation of subduction of the Rivera plate from 2.6–1.0 Ma, after which normal convergence resumed at a rate of ~3.2 cm/yr (DeMets and Traylen 2000). It is possible that the initiation of volcanic activity ~1 Ma is related to the resumption of the Rivera plate subduction, although bimodal rhyolite and high-Ti basalt volcanism is not generally associated with subduction. Perhaps hundreds of kyrs are required after resumption of subduction before voluminous andesite volcanism can occur.

Discrete eruptive episodes at arc stratovolcanoes

Ar chronology allows eruption time scales to be obtained not only for entire volcanic fields over a 1 Myr period but also for individual stratovolcanoes over relatively narrow intervals (tens of kyrs). At V. Tequila, six samples taken from different parts of the main edifice all have ages within two sigma of each other, leading to a mean eruption age of 196±12 ka. Therefore, the main edifice (~31 km^3) may have erupted within $\leq$24 kyrs (at the 95% confidence level), leading to an eruption rate of $\geq$1.3 km^3/kyr. However, we do not know the age of the earliest flows, which are covered. After a hiatus of ~110 kyr, a second eruptive episode began in which ~15±4 km^3 of andesite erupted along the W and SE flanks of V. Tequila at ~90±19 ka. The evidence for two discrete eruptive events is similar to what has been found at V. Ceboruco, ~75 km to the northwest (Frey et al 2004).

V. Ceboruco produced a caldera-forming eruption ~1000 years ago (Nelson 1980; Gardner and Tait 2000). Dates on the pre-caldera edifice indicate an initial cone-building episode ~50 kyr ago that erupted ~38 km^3 of two-pyroxene andesite (Frey et al 2004). The youngest pre-caldera activity (a vertical dike that cuts the uppermost flows) has been dated at 45±8 ka (Frey et al 2004). After a hiatus of ~44 kyr, a second major eruptive episode began with the caldera-forming eruption, which released 3–4 km^3 of dacite (Gardner and Tait 2000). Effusive eruptions of ~5.2 km^3 of andesite and ~4.4 km^3 of dacite have occurred since the Plinian eruption 1 kyr ago,

leading to a cone-building rate of ~9.6 km^3/kyr (Frey et al 2004). If this cone-building rate is applied to the pre-caldera edifice, then the first cone-building episode at V. Ceboruco may have lasted only ~4 kyr.

The data from V. Tequila and V. Ceboruco support the idea that some arc stratovolcanoes grow in spurts, namely short time intervals characterized by high eruption rates, which are separated by longer time intervals of little or no activity from the central vent. Hildreth and Lanphere (1994) showed that the Mt. Adams central vent in the Cascade arc was the site of three discrete cone-building events, each lasting $\leq$30 kyrs. The first hiatus lasted ~50 kyrs, whereas the second lasted ~400 kyr. The short time intervals over which arc cone-building episodes occur are demonstrated at several historically active stratovolcanoes. For example, the entire edifice of Arenal volcano in Costa Rica was erupted in the last ~2.9 kyrs (Borgia et al 1988), the composite Ngauruhoe volcano (~2.2 km^3) in New Zealand was erupted in the last 2.5 kyrs (Hobden et al 2002), Mount St. Helens volcano in the Cascade arc erupted ~40 km^3 in the last 4 kyr (Mullineaux 1986) and the stratocone of V. Colima (~5 km^3) was erupted in the last 4.3 kyr (Luhr and Prestegaard 1988). Even more impressive is the evidence that most of the cone of Shastina (part of Mt. Shasta volcano in the Cascades arc) was erupted in 300 years (between 9700 and 9400 years ago; Miller 1980).

An outstanding question is: what is the cause of the hiatus between these short-lived, though productive, cone-building events? Is this a time of magma differentiation in an upper crustal chamber? Or is the hiatus a time when the magma chamber has crystallized to a granitoid? Documentation of remarkably young ages of granitoid xenoliths erupted in various Holocene lavas by U-Th dating of zircons (Bacon et al 2000; Lowenstern et al 2000) may provide support of the latter interpretation. For example, Bacon et al (2000) obtained a U-Th isochron age of 112±24 ka for a granodiorite block ejected during the Mt. Mazama climactic eruption ~7.7 ka in the Cascade arc. The zircon age from the granodiorite shows that a young pluton had solidified by ~112±24 ka in virtually the same location where a similarly large magma body later accumulated and later erupted explosively to form Crater Lake (Bacon et al 2000). Similarly, Lowenstern et al (2000) obtained U-Th zircon ages of ~90 ka and ~25 ka on two granitoid xenoliths in lavas erupted 1065 and 2000 years ago, respectively, from Medicine Lake volcano, California. $^{40}Ar/^{39}Ar$ spectra on K-feldspar from the same granitoids indicate that they were sub-solidus by ~20 ka and ~10 ka, respectively. These are minimum argon ages owing to the possibility that they were partially re-set during entrainment in the host magma. Therefore, the maximum lengths of time in which these two granitoid magmas were partially molten at depth are $\leq$~70 kyr and $\leq$~15 kyr, respectively (Lowenstern et al 2000). The concept of relatively short-lived magma chambers beneath arc stratovolcanoes is further supported by plagioclase residence times of <1000 years in magmas, based on Sr trace element and isotopic diffusion systematics (Zellmer et al 1999; Davidson et al 2001).

Further evidence for two short-lived magma chambers separated in time and space

The $^{40}Ar/^{39}Ar$ chronologic evidence for two discrete magma chambers beneath V. Tequila, separated in time by ~110 ka, is further supported by phase equilibrium data. Most of the lavas erupted at ~90 ka along the western flanks of V. Tequila are distinguished from those erupted at ~200 ka from the main edifice by the addition of hornblende to an otherwise similar phenocryst assemblage of plagioclase and two pyroxenes (Tables 1a–1d, 2, 3, 4). The presence of hornblende phenocrysts in the andesites is unrelated to silica content; it occurs in western flank lavas with 58 to 64 wt% SiO_2. Wallace and Carmichael (1994) performed a petrologic study of both sets of lavas and show a systematic difference in their pre-eruptive temperatures and water concentrations. On the basis of both iron oxide and two-pyroxene thermometry, they calculated temperatures of ~910–950 °C for the hornblende-bearing, western flank andesites and ~990–1045 °C for the hornblende-free, main edifice andesites. Wallace and Carmichael (1994) used these temperatures in conjunction with the plagioclase-melt (Na-Ca exchange) equilibria of Housh and Luhr (1991) to estimate pre-eruptive water concentrations in the two groups: 4.0–4.1 wt% for the western flank andesites, and 2.5–2.8 wt% for the main edifice flows. These results are plotted in Fig. 6 for the seven andesites studied by Wallace and Carmichael (1994); two are from the main edifice, two are from the younger W flank, and three are from the younger SE flank. Surprisingly, the data show no correlation between silica concentration and either temperature (Fig. 6a) or water concentration (Fig. 6b). However, there is a correlation between the temperature and the amount of H_2O recorded by the phenocryst assemblages (Fig. 6c).

We combined the temperature and H_2O results with the experimentally determined water-saturated phase diagram of Moore and Carmichael (1998) for an andesite (similar to those erupted from V. Tequila). The andesites from the main edifice have temperatures (990 and 1045 °C) and water contents (~2.8 and ~2.5 wt%, respectively) that are consistent with a depth of equilibration of 50–70 MPa (~2–3 km) under fluid-saturated conditions (with H_2O the dominant fluid component) (Fig. 7). This *P-T* position places them <50° below the liquidus of plagioclase, which is consistent with their plagioclase abundances of ~15–20 vol% (Tables 1a–1d, 2, 3, 4; Moore and Carmichael 1998). If these andesites (with the same temperatures and water concentrations) crystallized under water-undersaturated conditions at higher pressures, then the shift to a positive dP/dT liquidus slope for plagioclase would lead to a significantly higher modal abundance of plagioclase than is observed.

Similarly, the younger flank lavas on the western side of V. Tequila have temperatures (912 and 958 °C) and

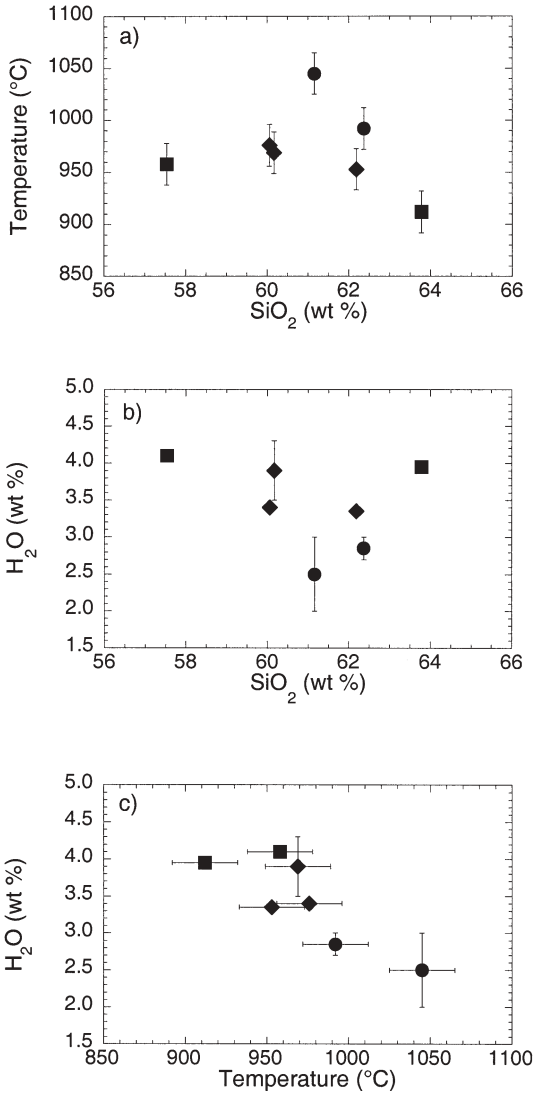

Fig. 6 a Plot of temperature versus silica content for Tequila andesites from Wallace and Carmichael (1994). Temperatures are based on two-pyroxene and/or Fe-Ti oxide thermometry. Solid dots are from the main edifice, solid squares are from the W flanks, and the solid triangles are from the SE flanks. **b** Same as in **a**, but wt% H_2O versus silica content. Wt% H_2O is based on Ca-Na exchange between plagioclase and liquid. Symbols are the same as in **a**. **c** H_2O versus temperature for the same lavas as in **a** and **b**

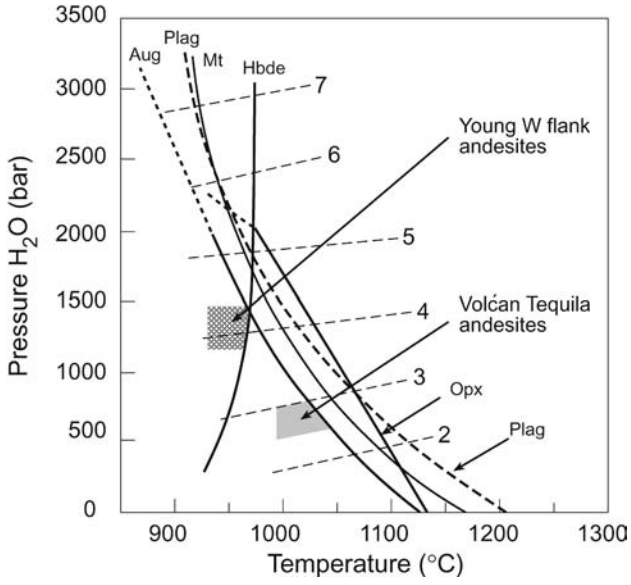

Fig. 7 Water-saturated phase diagram for an andesite, modified from Moore and Carmichael (1998). The dashed lines are isopleths of wt% water calculated from Moore et al (1998). The shaded areas indicate the *P-T* conditions of two magma chambers beneath V. Tequila, separated in time by ~110 kyrs

water concentrations (4.0 and 4.1 wt%, respectively) that place them at pressures of ~120–140 MPa (5–6 km) under fluid-saturated conditions (with H_2O the dominant component). Their plagioclase modal abundance of ~11–18 vol% also constrain them to be <50° below the plagioclase liquidus, which precludes water-undersaturated conditions at signficantly higher pressures. The younger SE flank lavas have slightly higher temperatures (953–976 °C) and slightly lower water concentrations (3.4–3.9 wt%). The correlation between the H_2O concentrations and the temperatures recorded in the phenocryst assemblages of all three groups of andesites (main edifice, W flank, SE flank) (Fig. 6c) is readily explained if crystallization is driven by degassing upon decompression (Moore and Carmichael 1998; Cashman and Blundy 2000; Metrich et al 2001; Carmichael 2002). An ascending, fluid-saturated (with H_2O the dominant component) andesite liquid at 950 versus 1050 °C will intersect the plagioclase liquidus curve at ~200 versus ~100 MPa (Fig. 7). Because water solubility increases with pressure, plagioclase grown at higher pressures will record higher dissolved H_2O contents than those grown at lower pressures.

In summary, it appears that the magma chamber that fed the eruptions of V. Tequila at ~200 ka was located at a relatively shallow depth of ~2–3 km (~50–70 MPa) and was injected by fluid-saturated magmas $\geq$990 °C. The absence of hornblende phenocrysts reflects these higher temperatures, which are above the thermal stability limit of hornblende. In contrast, a second chamber, which fed the western flank lavas ~110 kyrs later, appears to have been located at ~5–6 km depth and injected by cooler (910–960 °C), fluid-saturated magmas, allowing hornblende to crystallize. Both eruptive episodes at V. Tequila (~200 ka and ~90 ka) produced lavas that span the same range of silica content (58–64 wt% SiO_2), despite systematic differences in their respective temperatures, dissolved water concentrations, and depths of phenocryst growth.

Central versus peripheral eruptions of andesite and dacite

The location of the V. Tequila stratovolcano and the andesite flank lavas along a prominent NW-SE lineament suggests that they overlie a major passageway for mag-

mas ascending from the lower or middle crust. It is therefore not surprising that significant accumulations of magma occurred, leading to the formation of a magma chamber during at least two discrete time intervals. The two chambers that formed beneath V. Tequila are expected to have been the site of mingling between different ascending magma batches, which may or may not have been related to one another by crystal fractionation at depth. Ubiquitous disequilibrium textures in the lavas, described by Wallace and Carmichael (1994), confirm the mingling of at least three endmember magmatic compositions (andesite to dacite) prior to eruption. Importantly, the endmember magmas were already of andesitic to dacitic composition prior to their mingling within the upper crustal chambers beneath the stratovolcano.

The peripheral andesites and dacites, especially those erupted from the nine scoria and lava cones along the southern margin of V. Tequila, have very few phenocrysts, which suggests that they ascended rapidly through the upper crust and did not stall within an upper crustal chamber. There is no textural evidence for magma mingling, which is consistent with the monogenetic character of each cone and flow. The absence of an upper crustal chamber feeding these small-volume eruptions of andesite and dacite (total volume is ~2.4 km^3) is further supported by the distribution of their eruption ages over a 460 kyr interval (~685–225 ka), with no pattern of increasing silica content with time (Fig. 7).

The sparse phenocryst assemblage in the peripheral andesite and dacite lavas in the Tequila volcanic field, where there is little evidence of storage in a chamber, is suggestive that most hydrous andesitic and dacitic magmas are emplaced into the upper crust as crystal-poor *liquids* and that significant crystallization only occurs if they stall and degas within upper crustal chambers. The crystal-poor nature of the peripheral andesite and dacite lavas, along with the evidence of no upper crustal chamber feeding these eruptions, indicates that they had already attained their bulk composition prior to emplacement in the upper crust.

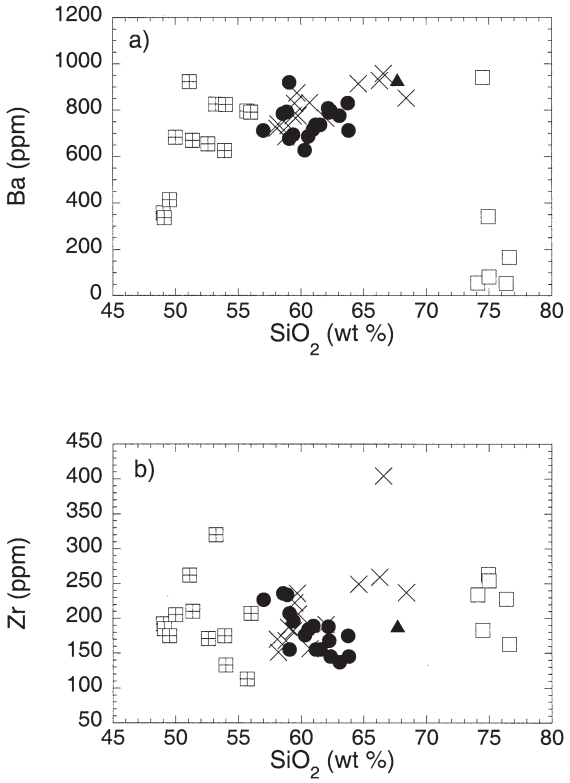

Fig. 8 a Plot of incompatible element Ba as a function of silica concentration for all samples, except ETZ-4, in Tables 1a–1d, 2, 3, 4 $\leq$1 Myr old. **b** Same as in **a**, but for incompatible element Zr. ETZ-4 is excluded owing to its exceptionally high concentrations of Ba and Zr. Basalts and basaltic andesites are shown by crosses enclosed by squares; andesites from the main edifice and flanks of V. Tequila are shown by solid dots; the dacitic pumice (TEQ23) is a solid triangle; andesites and dacites from peripheral scoria cones and flows are shown by the symbol ×; rhyolites are shown by open squares

Petrogenesis of lavas within the Tequila volcanic field

The eruptive chronology of the compositionally diverse lavas within the Tequila volcanic field, combined with their relative volumes, constrains models of their petrogenesis. Proposed models must be consistent with the following observations: (1) The basalts and rhyolites are broadly associated in time (1–0.2 Ma) and do not appear to be directly related to the voluminous eruptions of andesite over the last 200 kyrs. (2) There are no examples of mingled basalt and rhyolite magmas. (3) Less than 3 km^3 of andesite and dacite (59–69 wt% SiO_2) were erupted from small-volume, isolated flows and scoria cones over a period of ~460 kyrs (~685–225 ka) with no time progression in their compositions. (4) Andesite (predominantly 59–64 wt% SiO_2) was erupted in relatively large volumes (~31 and ~15 km^3, respectively) over relatively short intervals (tens of kyrs) at V. Tequila at two discrete times, separated by a hiatus of ~110 kyrs. (5) Hydrous andesitic and dacitic liquids were emplaced into the upper crust (either into short-lived chambers or directly onto the surface) as crystal-poor liquids.

Further constraints on the genetic relationships among the magmas are provided by simple plots of two incompatible trace elements, Ba (large ion lithophile) and Zr (high field strength) as a function of silica concentration (Fig. 8). The lavas are divided into four groups: (1) basalt/basaltic andesite, (2) andesite/dacite from V. Tequila and its flanks, including C. Tomasillo (PW-143 and PW-391 from Wallace and Carmichael 1994), (3) peripheral andesite/dacite, and (4) rhyolites. The basalts and basaltic andesites show a wide spread in these two incompatible elements and indicate considerable geochemical diversity among the mafic magmas. The rhyolites, with which the basalts are associated in time, have an equally large spread in Zr, and they range from peralkaline to metaluminous to peraluminous varieties (Harris 1986). They were therefore not all derived from a single, homogenous rhyolitic magma body with a long residence time in the

upper crust (~800 kyrs of eruptive history). A more plausible scenario is that rhyolitic domes and flows were produced during discrete episodes of partial melting of upper crust, most likely driven by the episodic emplacement of hot, basaltic magmas into the upper crust between 1.0 and 0.2 Ma; some of these basalts made it to the surface along NW-SE fractures and faults. It is unclear whether this bimodal volcanism of rhyolite and high-Ti basalt is a consequence of the renewed subduction of the Rivera plate ~1 Ma or whether it reflects regional extensional tectonics.

The andesites and dacites, especially those erupted in significant volumes from V. Tequila and its flanks, are not obviously linked to the basalts in terms of their eruptive history. If they are related by a crystal fractionation process to parental liquids similar to these more mafic lavas, then the scatter in Ba and Zr indicates that such a process must have operated on numerous parental liquids, each of which was geochemically distinct and likely of modest volume, following limited differentiation trends. This is similar to the conclusions drawn about magmas at the Tataro-San Pedro volcanic field by Dungan et al (2001) and at Crater Lake, Oregon (Bacon et al 1994; Bacon 1990; Bacon and Druitt 1988). Therefore, the image of a single or only a few large chambers of initially homogeneous magma undergoing crystal-fractionation is probably unrealistic. Nor is mixing of the rhyolites and basalts to produce the andesites and dacites a reasonable hypothesis because: (1) such mingled basalt/rhyolite lavas have not been identified in the Tequila volcanic field despite their coexistence for ~800 kyrs, (2) there is no evidence of a single olivine crystal in more than 150 thin sections of andesite/dacite lavas from the Tequila volcanic field examined petrographically by Wallace and Carmichael (1994) (and 28 more in this study), and (3) the textural evidence suggests that the andesitic and dacitic magmas were emplaced into the upper crust as homogenous, crystal-poor liquids and that mingling and significant crystallization occurred largely in upper crustal chambers. This third observation strongly argues against assimilation of granitoids by basalt to produce andesite/dacite, as the heat required to assimilate the granitoid would induce significant crystallization of the basalt, which in turn would not allow largely liquid andesite/dacite magmas to be produced.

Although several processes have been suggested to explain the origin of andesite at subduction zones, the evidence presented here can rule out, for the Tequila volcanic field, at least three commonly-invoked mechanisms: (1) magma mixing between rhyolite and basalt, (2) crustal assimilation of silicic granitoids by basalt, and (3) crystal fractionation of basalt to produce andesite/dacite in an *upper-crustal* chamber. It is more likely that the andesite and dacite erupted in the Tequila volcanic field were produced in the lower crust either by crystal fractionation of basalt (numerous different ones, each of modest volume) or partial melting of mafic amphibolite. Whatever mechanism is invoked to explain the generation of andesite at the Tequila volcanic field, it must be consistent with a bimodal distribution of high-Ti basalt and rhyolite for an 800 kyr interval beginning ~1 Ma, which abruptly switched to punctuated bursts of andesitic volcanism over the last 200 kyrs.

Acknowledgements This study was supported by NSF grant EAR-9909567. Thorough reviews by Anita Grunder, Charlie Bacon, and Julie Donnelly-Nolan significantly improved the manuscript. We thank Marcus Johnson for his assistance in the geochronology lab. We also thank Ian Carmichael for spending a few days with us in the field and for sharing his >30 years experience of the volcanic geology of western Mexico. We very much appreciate the field assistance of Marcos Luna Alonso and Miguel Angel Alatorre Ibarguengoitia. Discussions with Holli Frey about the ArcGIS software are also greatly appreciated. We especially thank Paul Wallace for sending us several samples from his collection, four of which were dated for this study.

References

Allan JF, Nelson SA, Luhr JF, Carmichael ISE, Wopat M, Wallace PJ (1991) Pliocene-Holocene rifting and associated volcanism in southwest Mexico: an exotic terrane in the making. In: Dauphin JP, Simoneit BA (eds) The gulf and peninsular province of the Californias. Am Assoc Petrol Geol Mem 47:425–445

Bacon CR (1990) Calc-alkaline, shoshonitic, and primitive tholeiitic lavas from monogenetic volcanoes near Crater Lake, Oregon. J Petrol 31:135–166

Bacon CR, Druitt TH (1988) Compositional evolution of the zoned calcalkaline magma chamber of Mount Mazama, Crater Lake, Oregon. Contrib Mineral Petr 98:224–256

Bacon CR, Gunn SH, Lanphere MA, Wooden JL (1994) Multiple isotopic components in quaternary volcanic rocks of the Cascade Arc near Crater Lake, Oregon. J Petrol 35:1521–1556

Bacon CR, Persing HM, Wooden JL, Ireland TR (2000) Late Pleistocene granodiorite beneath Crater Lake caldera, Oregon, dated by ion microprobe. Geology 28:467–470

Baksi AK, Archibald DA, Farrar E (1996) Intercalibration of $^{40}Ar/^{39}Ar$ dating standards. Chem Geol 129:307–324

Borgia A, Poore C, Carr MJ, Melson WG, Alvarado GE (1988) Structural, stratigraphic, and petrologic aspects of the Arenal-Chato volcanic system, Costa Rica: evolution of a young stratovolcanic complex. Bull Volcanol 50:86–105

Carmichael ISE (2002) The andesite aqueduct: perspectives on the evolution of intermediate magmatism in west-central (105–99°W) Mexico. Contrib Mineral Petr 143:641–663

Cashman K, Blundy J (2000) Degassing and crystallization of ascending andesite and dacite. Philos T Roy Soc A 358:1487–1513

Conway FM, Ferrill DA, Hall CM, Morris AP, Stamatakos JA, Connor CB, Halliday AN, Condit C (1997) Timing of basaltic volcanism along the Mesa Butte fault in the San Francisco volcanic field, Arizona, from $^{40}Ar/^{39}Ar$ dates: implications for longevity of cinder cone alignments. J Geophys Res 102:815–824

Crisp JA (1984) Rates of magma emplacement and volcanic output. J Volcanol Geoth Res 20:177–211

Damon PE, Nieto-Obregon J, Delgado-Argote LA (1979) Un plegamiento neogénico en Nayarit y Jalicso y evolución geomórphica del Río Grande de Santiago. Asoc Ing Min Met Geol Mex Memoria Técnica 12:156–191

Davidson J, Tepley III F, Palacz Z, Meffan-Main S (2001) Magma recharge, contamination and residence times revealed by in situ laser ablation isotopic analysis of feldspar in volcanic rocks. Earth Planet Sc Lett 184:427–442

Delgado-Granados H (1993) Late Cenozoic tectonics offshore western Mexico and its relation to the structure and volcanic

activity in the western Trans-Mexican volcanic belt. Geofis Int 32:543–559
Demant A (1979) Vulcanologia y petrografia del sector occidental del eje neovolcanico. UNAM Inst Geol Revista 3:39–57
DeMets C, Traylen S (2000) Motion of the Rivera plate since 10 Ma relative to the Pacific and North American plates and the mantle. Tectonophysics 318:119–159
DeMets C, Wilson DS (1997) Relative motions of the Pacific, Rivera, North American and Cocos plates since 0.78 Ma. J Geophys Res 102:2789–2806
Druitt TH, Edwards R, Mellors M, Pyle DM, Sparks RSJ, Lanphere MA, Davies M, Barriero B (1999) Santorini volcano (Geological Society Special Memoir 19). London Geol Soc, London, pp 1–165
Dungan MA, Wulff A, Thompson R (2001) Eruptive stratigraphy of the Tatara-San Pedro complex, 36°S, southern volcanic zone, Chilean Andes: reconstruction method and implications for magma evolution at long-lived arc volcanic centers. J Petrol 42:555–626
Frey HM, Lange RA, Hall CM, Delgado-Granados H (2004) Magma eruption rates constrained by $^{40}Ar/^{39}Ar$ chronology and GIS for the Ceboruco-San Pedro volcanic field, western Mexico. Geol Soc Am Bull 116:259–276 (Erratum 116:1040)
Gardner JE, Tait S (2000) The caldera-forming eruption of Volcán Ceboruco, Mexico. Bull Volcanol 62:20–33
Gilbert CM, Mahood GA, Carmichael ISE (1985) Volcanic stratigraphy of the Guadalajara area, Mexico. Geofís Int 24:169–192
Gill J (1981) Orogenic andesites and plate tectonics. Springer, Berlin Heidelberg New York, pp 1–385
Hall CM, Farrell JW (1995) Laser $^{40}Ar/^{39}Ar$ ages of tephra from Indian Ocean deep-sea sediments: tie points for the astronomical and geomagnetic polarity time scales. Earth Planet Sc Lett 133:327–338
Hall CM, York D (1978) K-Ar and $^{40}Ar/^{39}Ar$ age of the Laschamp geomagnetic polarity reversal. Nature 274:462–464
Hall CM, York D (1984) The applicability of $^{40}Ar/^{39}Ar$ dating to young volcanics. In: Mahaney WC (ed) Quaternary dating methods. Elsevier, Amsterdam, pp 67–74
Harris JM (1986) Silicic volcanics of Volcan Tequila, Jalisco, Mexico. MSc thesis, University of California, Berkeley, CA
Hildreth W, Lanphere MA (1994) Potassium-argon geochronology of a basalt-andesite-dacite arc system: the Mount Adams volcanic field, Cascade Range of southern Washington. Geol Soc Am Bull 106:1413–1429
Hildreth W, Fierstein J, Lanphere M (2003) Eruptive history and geochronology of the Mount Baker volcanic field, Washington. Geol Soc Am Bull 115:729–764
Hobden BJ, Houghton BF, Nairn AI (2002) Growth of a young, frequently active composite cone: Ngauruhoe volcano, New Zealand. Bull Volcanol 64:392–409
Housh TB, Luhr JF (1991) Plagioclase-melt equilibria in hydrous systems. Am Mineral 78:477–492
Hughes SS, Smith RP, Hackett WR, Anderson SR (1999) Mafic volcanism and environmental geology of the Eastern Snake River Plain, Idaho. In: Hughes SS, Thackray GD (eds) Guidebook to the geology of Eastern Idaho. Idaho Museum of Natural History, Pocatello, Idaho, pp 143–168
Klitgord KD, Mammerickx J (1982) Northern East Pacific Rise: magnetic anomaly and bathymetric framework. J Geophys Res 87:6725–6750
Lanphere MA (2000) Comparison of conventional K-Ar and $^{40}Ar/^{39}Ar$ dating of young mafic volcanic rocks. Quaternary Res 53:294–301
Lowenstern JB, Persing HM, Wooden JL, Lanphere M, Donnelly-Nolan J, Grove TL (2000) U-Th dating of single zircons from young granitoid xenoliths: new tools for understanding volcanic processes. Earth Planet Sc Lett 183:291–302
Luhr JF, Prestegaard KL (1988) Caldera formation at Volcano Colima, Mexico by a large holocene volcanic debris avalanche. J Volcanol Geoth Res 35:335–348
Mahood GA (1981) A summary of the geology and petrology of the Sierra La Primavera, Jalisco, Mexico. J Geophys Res 86: 10137–10152
Métrich N, Bertagnini A, Landi P, Rosi M (2001) Crystallization driven by decompression and water loss at Stromboli volcano (Aeolian Islands, Italy). J Petrol 42:1471–1490
Miller CD (1980) Potential hazards from future eruptions in the vicinity of Mount Shasta Volcano, northern California. USGS Bull 1503
Moore G, Carmichael ISE (1998) The hydrous phase equilibria (to 3 kbar) of an andesite and basaltic andesite from western Mexico: constraints on water content and conditions of phenocryst growth. Contrib Mineral Petr 130:304–319
Moore G, Venneman T, Carmichael ISE (1998) An empirical model for the solubility of water in magmas to 3 kbars. Am Mineral 83:36–42.
Mullineaux DM (1986) Summary of pre-1980 tephra-fall deposits erupted from Mount St. Helens, Washington State, USA. Bull Volcanol 48:17–26
Nelson SA (1980) Geology and petrology of Volcán Ceboruco, Nayarit, Mexico. Geol Soc Am Bull 91:2290–2431
Nelson SA, Livieres RA (1986) Contemporaneous calc-alkaline and alkaline volcanism in the region of Sangangüey volcano, Nayarit, Mexico. Geol Soc Am Bull 97:798–808
Nieto-Obregón J, Delgado L, Damon PE (1985) Geochronologic, petrologic, and structural data related to large morphologic features between the Sierra Madre Occidental and the Mexican volcanic belt. Geofís Int 24:623–663
Nixon GT, Demant A, Armstrong RL, Harakal JE (1987) K-Ar and geologic data bearing on the age and evolution of the Trans-Mexican volcanic belt. Geofís Int 26:109–158
Otsuki K (1989) Empirical relationships among the convergence rate of plates, rollback rate of trench axis and island-arc tectonics: laws of convergence rate of plates. Tectonophysics 159:73–94
Pardo M, Suárez G (1993) Steep subduction geometry of the Rivera plate beneath the Jalisco block in western Mexico. Geophys Res Lett 20:2391–2394
Renne PR, Swisher CC, Deino AL, Karner DB, Owens TL, DePaolo DJ (1998) Intercalibration of standards, absolute ages, and uncertainties in $^{40}Ar/^{39}Ar$ dating. Chem Geol 145:117–152
Samson SD, Alexander EC (1987) Calibration of the interlaboratory $^{40}Ar/^{39}Ar$ dating standard, Mmhb-1. Chem Geol 66:27–34
Singer BS, Thompson RA, Dungan MA, Feeley TC, Nelson ST, Pickens JC, Brown LL, Wulff AW, Davidson JP, Metzger J (1997) Volcanism and erosion during the past 930 k.y. at the Tatara-San Pedro complex, Chilean Andes. Geol Soc Am Bull 109:127–142
Steiger RH, Jäger E (1977) Subcommission on geochronology: convention on the use of decay constants in geo- and cosmochronology. Earth Planet Sc Lett 36:359–362
Taylor JR (1982) An introduction to error analysis: the studies of uncertainty in physical measurements. University Science Books, Mill Valley, CA, pp 1–270
Urrutia-Fucugauchi J, Flores-Ruis JH (1996) Bouguer gravity anomalies and regional crustal structure in central Mexico. Int Geol Rev 38:176–194
Wallace PJ, Carmichael ISE (1994) Petrology of Volcán Tequila, Jalisco, Mexico: disequilibrium phenocryst assemblages and evolution of the subvolcanic magma system. Contrib Mineral Petr 117:345–361
Wallace PJ, Carmichael ISE, Righter K, Becker TA (1992) Volcanism and tectonism in western Mexico: a contrast of style and substance. Geology 20:625–628
Wopat MA (1990) Quaternary alkaline volcanism and tectonics in the Mexican volcanic belt near Tequila, Jalisco, southwestern Mexico. PhD dissertation, University of California, Berkeley, CA
Zellmer GF, Blake S, Vance D, Hawkesworth C, Turner S (1999) Plagioclase residence times at two island arc volcanoes (Kameni Islands, Santorini, and Soufriere, St. Vincent) determined by Sr diffusion systematics. Contrib Mineral Petr 136:345–357